Bioorganic Chemistry 125 (2022) 105851

Contents lists available at ScienceDirect

Bioorganic Chemistry

journal homepage: www.elsevier.com/locate/bioorg

1*H*-imidazo[4,5-f][1,10]phenanthroline carbohydrate conjugates: Synthesis, DNA interactions and cytotoxic activity

Patricia Gratal [a,b], María-Selma Arias-Pérez [a,*], Lourdes Gude [a,b,*]

[a] Universidad de Alcalá, Departamento de Química Orgánica y Química Inorgánica, Grupo DISCOBAC, 28805-Alcalá de Henares, Madrid, Spain
[b] Universidad de Alcalá, Instituto de Investigación Química "Andrés M. del Río" (IQAR), 28805-Alcalá de Henares, Madrid, Spain

ARTICLE INFO

Keywords:
Carbohydrate conjugates
2-aryl-imidazo[4,5-f][1,10]phenanthroline derivatives
G-quadruplex DNA ligands
DNA interactions
Antitumor agents

ABSTRACT

Here we present a novel family of carbohydrate conjugates based on the 2-aryl-imidazo[4,5-f][1,10]phenanthroline core modified with carbohydrates (carb-APIPs). The hybrid compounds were prepared by direct treatment of the unprotected carbohydrate with 2-(4-**a**mino**p**henyl)-1*H*-**i**midazo[4,5-f][1,10]**p**henanthroline (APIP). The *N*-glycosylation reactions with the monosaccharides tested afforded stereoselectively the more stable *N*-β-glycopyranosylamines that, in solution, underwent a dynamic equilibrium leading to anomeric mixtures with a small participation of the α isomer. DNA interaction experiments with telomeric G-quadruplex DNA included DNA FRET melting assays, circular dichroism, and equilibrium dialysis and revealed that the novel carb-APIPs bind the G-quadruplex structure with high affinity. Interestingly, the presence of the carbohydrate confers good selectivity towards the telomeric quadruplex structure, as suggested by competition DNA FRET melting assays. Besides the extended aromatic surface that allows π-stacking interactions, the carbohydrate part of the conjugate may contribute to groove binding recognition, as indicated by viscosity experiments. In addition, the novel carb-APIPs showed significant cytotoxic properties in PC3 and HeLa cells and, to a lesser extent, in MCF7 cells and normal human fibroblasts (HFF1).

1. Introduction

The development of multifunctional compounds with high biosafety and multimodal therapeutic performance is currently a very active and competitive area of research. An essential aspect in this field is the possibility of modulating the properties of these derivatives throughout structural variations in several frameworks in an attempt to provide synergistic effects of the different active domains with sequential or supplementary activities. Among the diverse strategies so far explored, those based on biologically derived systems have been emerging as a privileged approach. Within this context, the incorporation of imidazole derivatives or carbohydrate subunits is particularly effective to control the biocompatibility and functions of multitarget compounds owing to their characteristics and structural variety [1,2].

Imidazole-based compounds have attracted considerable interest for their versatile properties in chemistry and the broad spectrum of biological activities. Imidazole core is ubiquitous in nature and develops a critical function in many structures, such as nucleic acids or metalloproteins and synthetic bioactive derivatives, with a whole range of medicinal chemistry applications as antiviral, antifungal, antibacterial or anticancer agents [1]. For example, veliparib and other poly(ADP-ribose) polymerase (PARP) inhibitors have arisen as promising biomarkers and anticancer therapeutics [3]. Particularly, imidazophenanthroline derivatives (IPs) play a key role in the implementation of a wide variety of multifunctional compounds and are receiving growing attention [1,4–8]. They are excellent chelating ligands that can form stable complexes with d-block transition metals and lanthanide ions. Imidazophenanthroline analogues and their metal complexes have been found to be ideal DNA probes due to their diverse DNA-binding modes, efficient DNA photocleavage effects and prominent photophysical and electrochemical properties [4–8]. These compounds have proved their ability to bind biologically relevant DNA structures, particularly quadruplex DNA, showing different degrees of selectivity. They can interact with G-4 DNA by end π-stacking and/or groove binding with high affinity. In addition, they can induce the stabilization of G-4 DNA in oncogenic promoters and at telomeres, which closely relates to the regulation of gene expression and inhibition of telomerase activity, as well as to their therapeutic potential in cancer chemotherapy [9,10]. It

* Corresponding authors at: Universidad de Alcalá, Departamento de Química Orgánica y Química Inorgánica, Grupo DISCOBAC, 28805-Alcalá de Henares, Madrid, Spain (L. Gude).
E-mail addresses: selma.arias@uah.es (M.-S. Arias-Pérez), lourdes.gude@uah.es (L. Gude).

https://doi.org/10.1016/j.bioorg.2022.105851
Received 7 February 2022; Received in revised form 5 April 2022; Accepted 29 April 2022
Available online 6 May 2022

has been found that diverse sets of IPs exhibited cytotoxic activities and inhibitory selectivity against several human cancer cell lines but with low toxicity towards normal cells [4–7]. Other mechanisms have also been described to elucidate the anticancer activities of these compounds based on the inhibition of DNA synthesis or DNA photocleavage via formation of reactive oxygen species [5–7]. In addition, they have also been proposed as fluorescence molecular probes for cellular imaging and cancer screening studies due to their prominent optical properties [4–7]. Other applications include their use as dyes and functional materials, such as electrochemical DNA biosensors, organic light-emitting diodes (OLEDs) [4–6,8].

On the other hand, carbohydrates currently play a significant role in medical chemistry and chemical biology [2,11,12]. The intracellular uptake in tumor cells can be ensured by appending sugars on multivalent derivatives by taking advantage of the "Warburg effect" and energy requirements displayed by cancerous cells, which would greatly enhance the targeting efficacy of an anticancer agent [13]. In addition, it is well known that many carbohydrates are good binders for nucleic acids in general, and for G-quadruplexes in particular. Recent studies on sugar-DNA conjugates highlight the fact that carbohydrates are able to bind G-quadruplexes through stacking interactions as well as hydrogen bonding or hydrophobic contacts involving the grooves and/or loops, which can further stabilize these secondary structures [14–16]. Moreover, several carbohydrate-functionalized derivatives have been proven to be excellent G-quadruplex ligands and/or exhibit relevant antitumor activity, which makes them interesting compounds from the perspective of anticancer therapies [14–16].

Bearing in mind that selective G-quadruplex ligands offer great promise for anticancer drugs development [9,10], we are interested in the preparation of carbohydrate conjugates based on heteroaromatic systems acting as bidentate metal chelators and DNA intercalating agents. We have shown that the *N*-(1,10-phenanthrolin-5-yl)-β-glycopyranosylamine and N^1-(4,5-diazafluoren-9-yliden)-N^2-glycopyranosyl hydrazine copper(II) complexes can bind DNA sequences and preferentially stabilize G-quadruplex DNA structures over dsDNA [15b,15c]. Moreover, several complexes exhibited a cytotoxic activity against cultured HeLa and PC3 tumor cells comparable to other metal complexes normally used for chemotherapeutic purposes, such as cisplatin [15c]. Herein, we describe the synthesis and characterization of a novel series of *N*-4-(1*H*-imidazo[4,5-f][1,10]phenanthrolin-2-yl)phenyl-β-glycopyranosylamines (carb-APIPs, Scheme 1), as well as their DNA interactions and cytotoxic activity. These ligands have several important features, which are favorable for developing efficient DNA binding and anticancer agents. The extended planar aromatic imidazophenanthroline backbone and the extra π-conjugation with the aryl moiety leads to a potentially better π-stacking and higher active component compared to the 1,10-phenanthroline or 4,5-diazafluorene systems set out in our previous studies, suggesting that the selected derivatives may be able of binding quadruplex structures (G4s) on their own, [9,10] even in the absence of a metal, unlike the previously reported derivatives [15b,15c]. Moreover, it is well-documented that 1*H*-imidazo[4,5-f][1,10]phenanthroline-based ligands are efficient binders of quadruplex DNA structures [4,6,7]. These new *N*-heteroaryl glycosylamines include a carbohydrate unit connected to the outer aryl system through a *N*-glycoside linker. By sugar conjugation we expected to increase compound solubility and bioavailability, incorporate an extra binding domain to increase interactions with G-quadruplexes and improve targeting efficacy, as well as promote the entry into the cell through specific sugar transporters [13–16]. Because carbohydrates can give rise to significant differences in the affinity for a quadruplex-target, we selected to attach different monosaccharides in order to obtain useful SAR information on the role the carbohydrate core plays in binding and its ability to raise additional interactions, as well as corroborate previous studies on related derivatives. The chosen carbohydrates (D-glucose, D-mannose, 2-deoxy-D-glucose, L-rhamnose, L-xylose), represent examples of monosaccharides from the D- and L-series, with different stereochemical arrangement and/or replacement of the OH groups. Moreover, they have exhibited relevant biological activities as key structural units in antitumor agents and vaccines [2,11,12]. In addition, glycosylamines are key players in carbohydrate enzymology, as they can act as inhibitors of glycosidases [17]. For example, antitumor indolocarbazole *N*-glycosides such as rebeccamycin analogues can inhibit topoisomerases, kinases and/or bind to DNA [18].

In addition to the preparation of the novel carb-APIPs and their structural characterization, an initial study of DNA interactions has been carried out on the human telomeric G-quadruplex structure Tel22 as a potential DNA target. Different techniques have been employed for this purpose, which include fluorescence-based assays (non-competitive and competitive DNA FRET melting assays), circular dichroism and equilibrium dialysis experiments. Furthermore, viscosity assays with dsDNA have been used as well to establish their general DNA binding behavior as π-stacking/intercalating or/and groove binding agents. Finally, a preliminary evaluation of cytotoxic activity against a panel of cultured tumor cells is also included in this work.

2. Results and discussion

2.1. Synthesis and structural study

The *N*-glycosylation reactions were carried out by direct treatment of the unprotected carbohydrate with 2-(4-aminophenyl)-1*H*-imidazo[4,5-f][1,10]phenanthroline [15a,19]. After dehydration of the tetrahedral intermediate, the reactive electrophilic imine sets the stage for intramolecular cyclization to afford generally the corresponding thermodynamically-favored cyclic *N*-glycoside. The best results were obtained using a large excess of carbohydrate (3 equiv.) and a catalytic amount of $(NH_4)_2SO_4$ as promotor in methanol, as was previously described for the synthesis of *N*-(1,10-phenanthrolin-5-yl)-

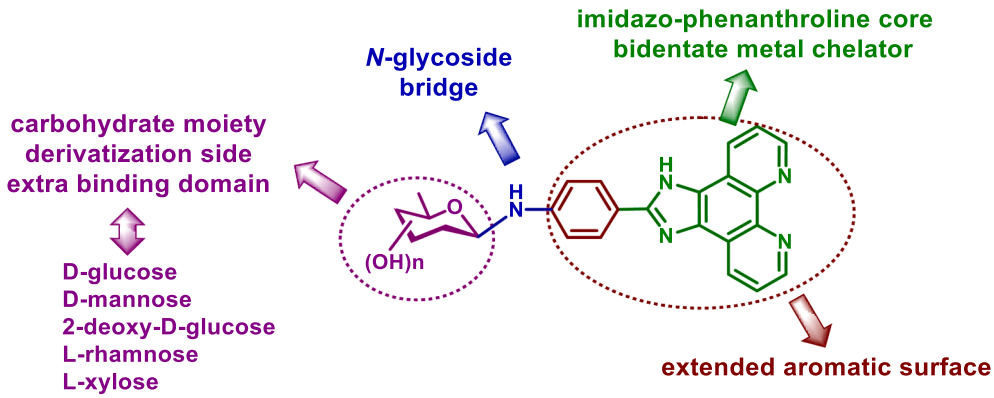

Scheme 1. Structure of the 2-(4-aminophenyl)-1*H*-imidazo[4,5-f][1,10]phenanthroline carbohydrate conjugates (carb-APIPs).

β-glycopyranosylamines [15a]. At 60 °C for 24 h the conversion of the starting amine **2** was practically quantitative and the reactions with the monosaccharides tested afforded the *N*-β-glycopyranosylamines **3a-e** in synthetically useful yields (78–84%, Scheme 2); when the process was carried out in the absence of catalyst the yields were lower (ca. 60–70%). Decomposition, hydrolysis and/or other by-products were not detectable in yields higher than 3%. Thermodynamics is a major driving force in determining anomeric stereoselectivity, which is strongly influenced by the steric features of the amine and the sugar. The high stereoselectivity of the process could be explained on the basis of the greater stability of the β anomer, with an equatorial disposition of the anomeric group, owing to the contribution of the reverse anomeric effect and the *exo*-anomeric interactions that control the conformational preferences of the nitrogen glycosides. For *N*-arylglucopyranosylamines it was described that accentuated steric interactions associated with the *exo*-anomeric effect were operative in the axial isomer, thereby favoring the equatorial one [20]. Moreover, this trend may be enhanced for aglycons with a greater bulk near to the point of glycosylation.

The carb-APIP derivatives **3a-e** were studied in depth by ^{1}H and ^{13}C NMR in $(CD_3)_2SO$, using homonuclear and heteronuclear 2D-NMR techniques for the identification and unambiguous assignment of the proton and carbon resonances (Figures S1-S22). At 500 MHz the ^{1}H NMR spectra showed greater complexity in the region around 3.0–5.1 ppm, where most signals of the saccharide moieties appear. Addition of D_2O facilitated the identification of acidic OH and NH proton resonances and the study of the remaining signals since, in these conditions, the vicinal coupling constants with OH and NH protons were removed. The interpretation of the ^{1}H–^{1}H COSY and ROESY spectra was based on the unambiguous assignment of the signals corresponding to the anomeric protons (H-1) and the 6-OH protons (apparent triplet) in **3a-c**, CH_3-6 groups in **3d** or cyclic CH_2 protons in **3c,e** owing to their shape and chemical shifts. The bridge NH proton was observed as a doublet around 7.0–6.2 ppm, while imidazolyl NH proton appeared as a singlet about 13.4 ppm. Aromatic protons of amine **2** and *N*-glycosides **3a-e** resonate around 9.0–6.7 ppm, showing very similar chemical shifts. The unequivocal assignment of all carbon resonances was based on the chemical shifts observed in related systems and the analysis of the direct and long-range ^{1}H–^{13}C correlated spectra (gC2HSQCSE, gHMBC), once the signals of the respective protons were established. Chemical shifts and shape of the phenanthroline proton signals are dependent on the solvent and concentration; H-4″/H-11″ as well as H-5″/H-10″ and H-6″/H-9″ (see scheme 2 for numbering) become chemically equivalent in **2**, however usually appear as discrete signals without degeneracy, although with subtle but detectable Δδ. in derivatives **3a-e**. Concerning the carbon atoms, the imidazo[4,5-f][1,10]phenanthroline group gives broadened and weak signals -except C-2″ quaternary imidazole carbons beyond detection in some cases- that were more easily identified in the ^{1}H–^{13}C correlation 2D spectra (gC2HSQC, gHMBC, Figures S3, S8 and S9). This behavior suggests an intermediate exchange rate for the imidazole prototropic taumerism [8b,21] and a small influence of the carbohydrate moiety, probably due to the existence of different hydrogen bond networks in **2** and the *N*-glycosylamines. For all compounds, the carbons of the substituted aryl group attached to the imidazophenanthroline system gave sharp signals. Data are collected in Table 1 and in the Experimental section.

The *N*-glycosylamines generally adopt a cyclic structure predominating pyranose forms, which can exist in solution as dynamic equilibrium mixtures of two possible anomers (α/β) by a thermodynamic balance between the open imine-type intermediate and closed ring forms. The composition of the equilibrium depends largely on the solvent, the nature of the carbohydrate and the aglycon, along with the basicity of the compounds. Usually, the β anomer is favored due to its greater stability and the tendency for equatorial orientation of the anomeric group is so strong that is the unique form detected for some derivatives. This is the case of the *N*-(1,10-phenanthrolin-5-yl)-β-glycopyranosylamines in which the phenanthroline moiety is directly connected to the anomeric carbon by the *N*-glycosidic atom [15a]. The solution equilibrium between both anomers has been put forth as a potential advantage in the context of bioactivity, where binding of one isomer to a biological target would help drive the equilibrium towards the bioactive form.

The NMR spectra of the carb-APIPs **3a-e,** recorded using freshly prepared samples in $(CD_3)_2SO$, provide conclusive evidence that these derivatives adopt *N*-glycopyranoside structure and exist practically as a single anomer [15a,19f,19g,19i,20]. The anomeric configuration could be readily inferred from NOE experiments (2D ROESY spectra). The NOE correlations between H1 and H-3/H-5 protons in all cases (Scheme 2) and between H1 and the equatorial H-2 in **3b-d** indicate an axial orientation of the anomeric proton (Figure S13 for **3b**). The large vicinal coupling constants (10.7–8.2 Hz, Table 1) between H-1 and the H-2 in **3a,c,e** corroborate their *trans*-diaxial relationship proving the equatorial disposition of the anomeric group. These features as well as anomeric proton and carbon chemical shifts and the ^{13}C–^{1}H direct coupling constant for the C-1 carbon ($^{1}J_{CH}$ = 150 Hz, Table 1) are in agreement with the β anomeric configuration [15a,20a]. The experimental values of the vicinal proton coupling constants of the pyranoside ring revealed that the D-glycosides **3a-c** adopt exclusively the $^{4}C_1$ conformation and the L-glycosides **3d,e** the $^{1}C_4$ form in $(CD_3)_2SO$ or $(CD_3)_2SO/D_2O$ solutions. The large values of coupling constants $^{3}J_{NH\text{-}H1}$ (9.5–7.6 Hz, Table 1) are consistent with a near *anti* relationship between NH and H-1 in $(CD_3)_2SO$

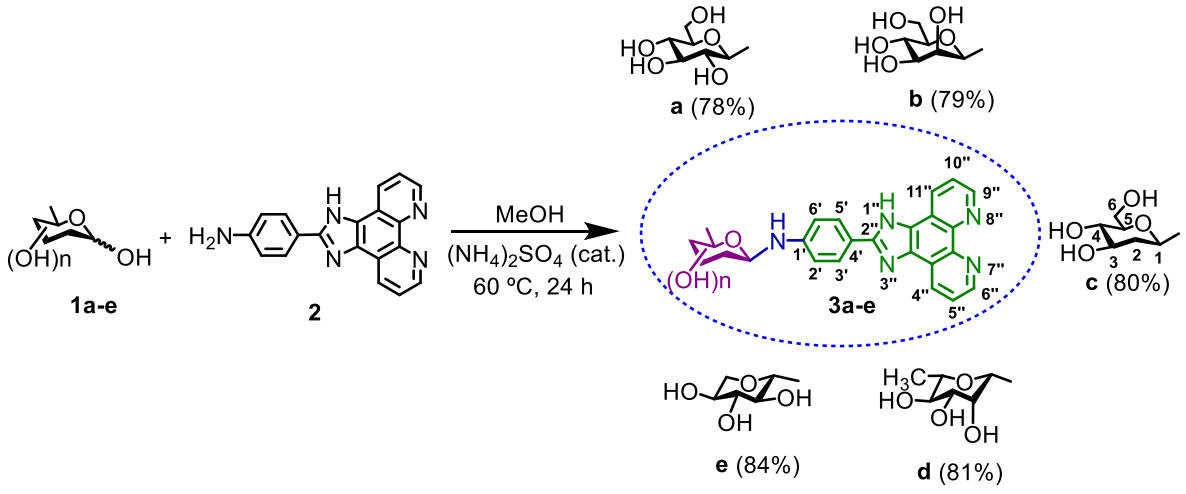

Scheme 2. Synthesis of the carb-APIPs **3a-e.**

Table 1
Selected NMR parameters of the *N*-aryl-imidazo[4,5-f][1,10]phenanthroline glycosylamines (carb-APIPs) **3a-e** in $(CD_3)_2SO$.

	2	3aβ (α)	3bβ (α)	3cβ (α)	3dβ (α)	3eβ (α)
δ (ppm)						
H-1		4.50(5.02[a])	4.87 (4.97[a])	4.81 (5.18)	4.87 (4.94)	4.47 (5.00[a])
bH	5.64	6.77	6.31 (6.85)	6.95 (6.94)	6.23 (6.85)	6.75 (6.46)
H-2′(6′)	6.74	6.90	6.97	6.87	6.96 (6.98)	6.88
H-3′(5′)	7.97	8.05	8.04	8.04	8.04 (8.05)	8.05
H-5″(10″)	7.81	7.80; 7.84	7.80; 7.84	7.80; 7.84	7.81; 7.85	7.80; 7.84
C-1		84.4	81.1	79.7 (78.4)	80.8 (83.2)	85.0 (80.7)
C-1′[b]	152.1	148.8	147.9	148.2	147.9	148.5
J (Hz)						
$^3J_{H1\text{-}H2}$		8.6 (4.9[a])	- (1.8[a])	10.7;1.5 (4.9)	- (1.5)	8.2 (4.0[a])
$^3J_{H1\text{-}NH}$		7.6	9.5 (5.3)	8.3 (5.5)	9.5 (6.1)	8.0 (6.5)
$^1J_{C1\text{-}H1}$		150	150	150 (155)	150 (160)	150 (155)

[a] Values in $(CD_3)_2SO$-D_2O.
[b] C-1′ is C-4′ in the starting amine **2**.

solution, probably due to a preferred conformation around C1-N bond stabilized by certain contribution of *exo*-anomeric interactions [15a,20a].

However, when the compounds were kept in $(CD_3)_2SO$ or $(CD_3)_2SO$/D_2O solutions it was found that β anomer underwent a slow interconversion to the α anomer leading to an equilibrium mixture of both isomers (Figure S17). In any case, the preference corresponds to the equatorially substituted isomer and the β/α ratio is dependent on the nature of the carbohydrate and the solvent. Thus, after 24 h in $(CD_3)_2SO/D_2O$ solutions the participation of the α anomer was about 10% for **3a**, 3% for **3b** and 20% for **3c-e**. These observations corroborate that the *N*-glycosylation occurred stereoselectively leading exclusively to the most stable *N*-β-glycoside that may be the solid-state structure, while any observed anomeric mixture is due to a dynamic solution equilibrium. The different behavior of derivatives **3** compared to the *N*-(1,10-phenanthrolin-5-yl)-β–glycopyranosylamines [15a] might be related to the different environment around the glycosidic bond: the phenyl ring moves away the bulky heteroaromatic system, leading to lower steric demand of the anomeric substituent [20].

2.2. DNA interactions

2.2.1. DNA FRET melting assays

In the study of DNA interactions, we first wanted to determine whether the series of carb-APIP compounds (**3a-e)** can efficiently bind DNA and, in particular, quadruplex DNA. As DNA target, the human telomeric sequence was chosen (Table 2), folded in the presence of potassium ions, which represents a mixture of hybrid structures. This quadruplex DNA was selected based on the wide structural information available of this polymorphic structure and its biological relevance in cancer biology [22].

FRET DNA melting assays were thus initially used to determine whether the carb-APIPs are able to thermically stabilize the telomeric quadruplex structure. For that purpose, oligonucleotide F21T labeled with the fluorophore FAM at its 5′ end and the fluorophore TAMRA at the 3′ end was employed [23a,23b]. In a similar fashion, in parallel experiments, interaction with oligonucleotide F10T was investigated as well, as a comparative measurement for duplex stabilization [23c]. Experiments were performed on folded (or annealed) DNA in the absence and in the presence of increasing concentrations of carb-APIPs **3a-e** and precursor amine **2** by slow heating from 25 °C to 95 °C. This allowed the determination of T_m values (precisely $T_{1/2}$ values)[23a] and to establish whether a significant variation of thermal stability of the secondary DNA structure is observed upon compound binding.

Table 2
DNA oligonucleotide sequences used to study carb-APIP-DNA interactions.

Name sequence	Type	Sequence (5′-3′)
Tel 22	G4 (telomeric)	5′-AGGGTTAGGGTTAGGGTTAGGG-3′
F21T	G4 (telomeric, Fl[a])	5′-FAM-GGGTTAGGGTTAGGGTTAGGG-TAMRA – 3′
F10T	dsDNA (Fl[a])	5′-FAM-TATAGCTATA/Sp18/TAGCTATA-TAMRA – 3′
ds26	dsDNA	5′-CAATCGGATCGAATTCGATCCGATTG-3′

[a] Fl = fluorescencently labeled.

The ability of a G4 ligand to stabilize quadruplex DNA, estimated by the modification of its melting temperature (ΔT_m), is usually reported at 1 μM compound concentration. In our experimental conditions, all carb-APIPs showed a very significant stabilization of the telomeric quadruplex, with ΔT_m values at the reference concentration ranging from ca. 7 to 12 °C (Fig. 1A). The higher stabilization results obtained for **3b** and **3d** (mannose and rhamnose derivatives, respectively) are comparable to those found with other well established quadruplex ligands tested under the same experimental conditions, such as, for example, compound 360A ($\Delta T_{1/2} \approx 12$ °C, at 1 μM) [15b]. Regarding the effect of ligand concentration, a direct correlation between concentration and G4 stabilization was observed, although the T_m increment observed was not regular for all compounds. At 1 μM, for example, the order of thermal stabilization observed for the carb-APIs was **3b** > **3d** > **3a** > **3e** > **3c**, with that meaning that the mannose derivative is the more efficient stabilizing ligand and the 2-deoxyglucose the less efficient. At a ligand concentration range between 2.5 and 4.5 μM the relative order of stabilizing ability between **3d** and **3a** (rhamnose and glucose, respectively) is reversed (Fig. 1A), although at the higher concentration, 5 μM, the rhamnose derivative **3d** showed again a higher ΔT_m value. In addition, up to a concentration of ~4 μM, compound **2** induced less stabilization of the telomeric quadruplex structure than the carb-APIPs, with the exception of compound **3c**. It is important to point out that these results clearly differ from those obtained with the family of *N*-(1,10-phenanthrolin-5-yl)-β-glycopyranosylamines, where no DNA thermal stabilization was observed unless the ligands were complexed with Cu(II), and even in that case, no appreciable thermal stabilization was observed until a 3 μM compound concentration was reached [15b]. In general, the new family of ligands, which include in their structure the imidazole and a phenyl ring, are much better G4 stabilizers than their *N*-(1,10-phenanthrolin-5-yl)-β-glycopyranosylamine counterparts, which can be explained in terms of their increased surface which might favor π-interactions with the telomeric quadruplex.

When compounds **3a-e** were tested for stabilization of double-stranded DNA, with the 10 bp sequence F10T (Fig. 1B), it was found that they were able to produce a modest stabilization of the labeled DNA duplex structure. At a concentration of 1 μM, all the carb-APIPs and compound **2** revealed low and relatively similar stabilization, with ΔT_m values of 2–3 °C. As compound concentration was increased, the stabilization profile differed slightly, showing that **3b**, **3d** and **3a** (containing mannose, rhamnose and glucose, respectively) can stabilize dsDNA to a

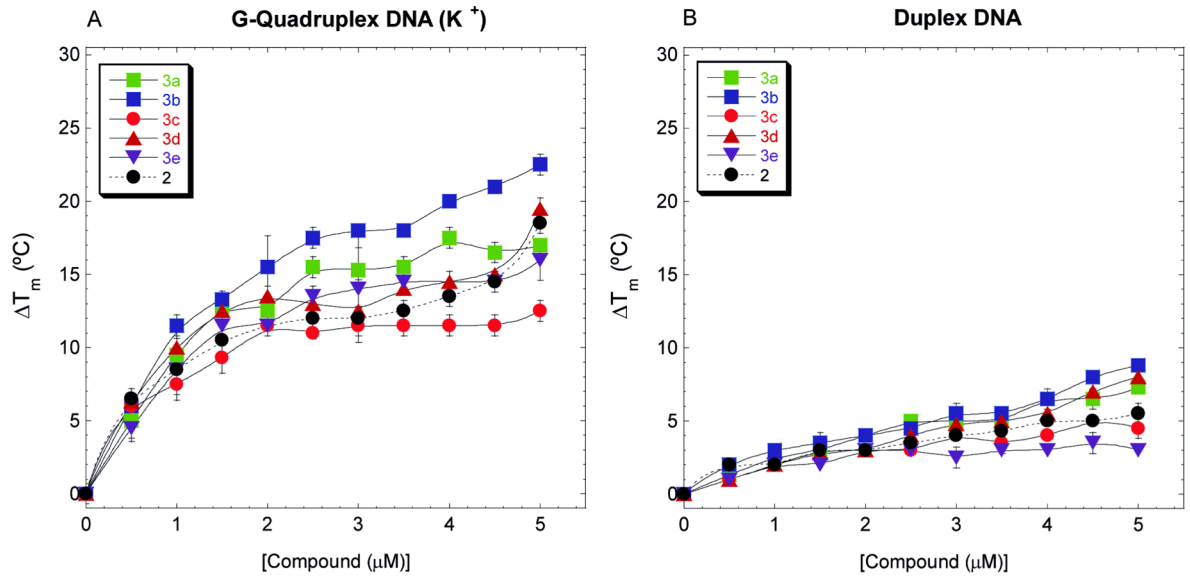

Fig. 1. DNA FRET melting experiments for compounds **3a-e** and **2** at a concentration range between 0 and 5 μM with A) telomeric oligonucleotide F21T (potassium buffer). B) duplex DNA F10T (sodium buffer).

greater extent than **3c** and, especially, over **3e** (bearing 2-deoxyglucose and xylose, respectively). Compound **2** displayed a modest stabilization of F10T, lower than compounds **3b**, **3d** and **3a**, but higher than that observed for compounds **3c** and **3e**. The interval of ΔT_m values at the higher concentration (5 μM) ranges from 3 to 9 °C with F10T, compared to 13 to 23 °C in the case of the quadruplex F21T DNA sequence. Taken together, these results may suggest the preferential binding and stabilization of the quadruplex DNA structure by the carb-APIPs. However, as the duplex F10T DNA displays higher thermal stability than quadruplex F21T, these finding should be taken with caution and additional experiments under real competition conditions should be considered.

Therefore, to address quadruplex versus duplex DNA selectivity, analogous melting experiments with F21T were repeated by maintaining the carb-APIP concentration equal to 5 μM, in the absence and in the presence of an unlabeled dsDNA competitive sequence, ds26. Following standard protocols, the competitive sequence was added at two different concentrations, 3 and 10 μM, which represent a considerably high duplex DNA stoichiometric excess (15-fold and a 50-fold, respectively). Afterwards, binding selectivity (S), at 3 and 10 μM, was determined according to the following equation: $S = (\Delta T_m)_{\text{with dsDNA competitor}} / (\Delta T_m)_{\text{without dsDNA competitor}}$. Compounds especially selective for quadruplex DNA structures are expected to maintain the ΔT_m values very similar to the values in the absence of duplex DNA, irrespective of the amount of dsDNA added. Thus, S values of 1 (or near to 1) represent high selectivity for the quadruplex DNA structure.

As previously mentioned, when the telomeric quadruplex F21T was incubated with carb-APIPs at 5 μM concentration, significant stabilization of the structure was observed (Fig. 2). Upon the addition of excess of the ds26 sequence at 3 and at 10 μM concentration, some of the compounds displayed an appreciable decrease in ΔT_m, such as **3b** (with mannose) and, to a letter extent, **3c** and **3a** (having 2-deoxyglucose and glucose, respectively). However, compounds containing xylose (**3e**) and, especially, rhamnose (**3d**) were able to maintain the ΔT_m values closer to the initial values, even at high excess of duplex DNA. This observation indicates that these two compounds are quite selective for quadruplex structure, in particular the rhamnose derivative. The values of

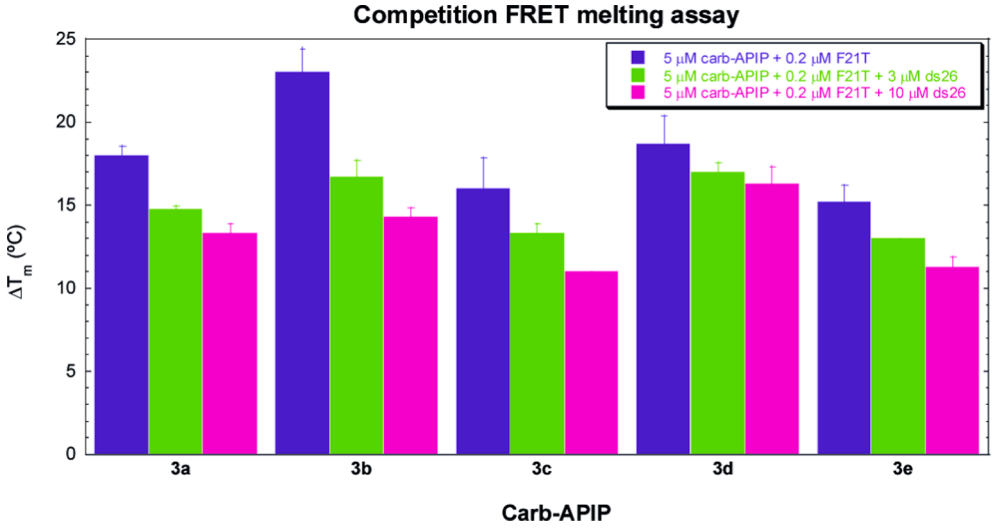

Fig. 2. Competition DNA FRET melting experiments for carb-APIPs **3a-e** at a 5 μM concentration with 0.2 μM G4 sequence F21T (10 mM lithium cacodylate, 90 mM LiCl, 10 mM KCl) in the absence (blue) and in the presence (green and pink) of competitor dsDNA sequence ds26: 3 μM, 15-fold dsDNA excess (green) and 10 μM, 50-fold dsDNA excess (pink). (For interpretation of the references to colour in this figure legend, the reader is referred to the web version of this article.)

selectivity (S) found were: 0.91 and 0.87 for **3d** and 0.86 and 0.74 for **3e**, at 3 and 10 μM of competitor, respectively (Table S1 in Supporting Information). S values for rhamnose derivative **3d** were found to be very close to those obtained with reference quadruplex ligand 360A (0.93 and 0.88, at 3 and 10 μM of competitor, respectively, Table S1 and Fig. S23A). In summary, selectivity determined by this assay was found to decrease in the order **3d** > **3e** > **3a** ≈ **3c** > **3b**. Finally, it is important to remark that the precursor amine, compound **2**, tested under the same experimental conditions, showed considerably lower selectivity values (S = 0.67 and S = 0.47, at 3 and 10 μM of competitor, respectively, Table S1 and Fig. S23B) than any of the carb-APIPs studied herein, which clearly indicates that the carbohydrate part of the ligand is exerting a significant contribution in quadruplex recognition, and conferring the compounds with quadruplex/duplex binding selectivity.

2.2.2. *Circular dichroism*

Next, the effect of the binding of carb-APIPs **3a-e** on the structure of the telomeric G-quadruplex sequence DNA, folded under potassium conditions, was qualitatively monitored by circular dichroism (CD). This technique allows the determination of characteristic folding topologies of G-quadruplexes as a function of metal ion and concentration, temperature, etc. or upon ligand binding [24,25].

In our experimental conditions, the CD spectrum of Tel22 was found to be consistent with previous data reported in the literature for a properly folded structure. The folding topologies for the studied quadruplex, a mixture of hybrid structures, belong to the group II topology [24b,24c]. In K^+ solution, Tel22 characteristic spectral properties are a positive signal around 295 nm with a shoulder at 270 nm, and a trough at 235 nm. These features are distinctive of mixed antiparallel-parallel quadruplex topology and, in the present case, confirms the existence of DNA hybrid (3 + 1) structures [26].

For the qualitative evaluation of the effects of the carb-APIPs on DNA structure, the CD spectra of G-quadruplex DNA, folded in the presence of K^+ at different molar ratios [ligand/DNA, from 0:1 up to 5:1], were recorded. Interestingly, several spectral modifications were observed, indicating that the carb-APIPs can induce changes in the conformation of Tel22.

As shown in Fig. 3 (Panel A), the glucose derivative **3a** gave rise to changes both in the 295 nm band and in the region ca. 240–270 nm. The intensity of the signal at 295 nm was slightly reduced as a function of an increase of compound **3a** concentration, whereas the wide region at 240–270 nm presented a considerable enhancement in ellipticity. This change may be suggestive of an increase in the parallel character of the structure. In the case of the compounds containing mannose and 2-deoxyglucose (**3b** and **3c**, Fig. 3, panels B,C), the intensity of the characteristic bands at 295 nm was reduced to a greater extent than in the case of compound **3a**, whereas the region 240–270 keeps the same signature as in Tel22 alone, with a slight ellipticity enhancement as compound concentration increases. However, **3c**, at the higher ligand to DNA ratio studied, produced a greater spectral modification at ~ 260 nm, an effect that resembles that observed for compound **3a**. The rhamnose derivative **3d** showed a clear increase in the intensity of the shoulder at 270 nm, while little effect on the band at 295 nm (Fig. 3D). Overall, compounds **3a-d** seem to stabilize the parallel-type topology at the ligand/DNA ratios examined. The xylose derivative **3e**, exhibited a more subtle modification of the CD spectrum of the telomeric quadruplex, which reflects that its binding is not producing important structural changes (Fig. 3E). Moreover, this compound showed a concentration-dependent,

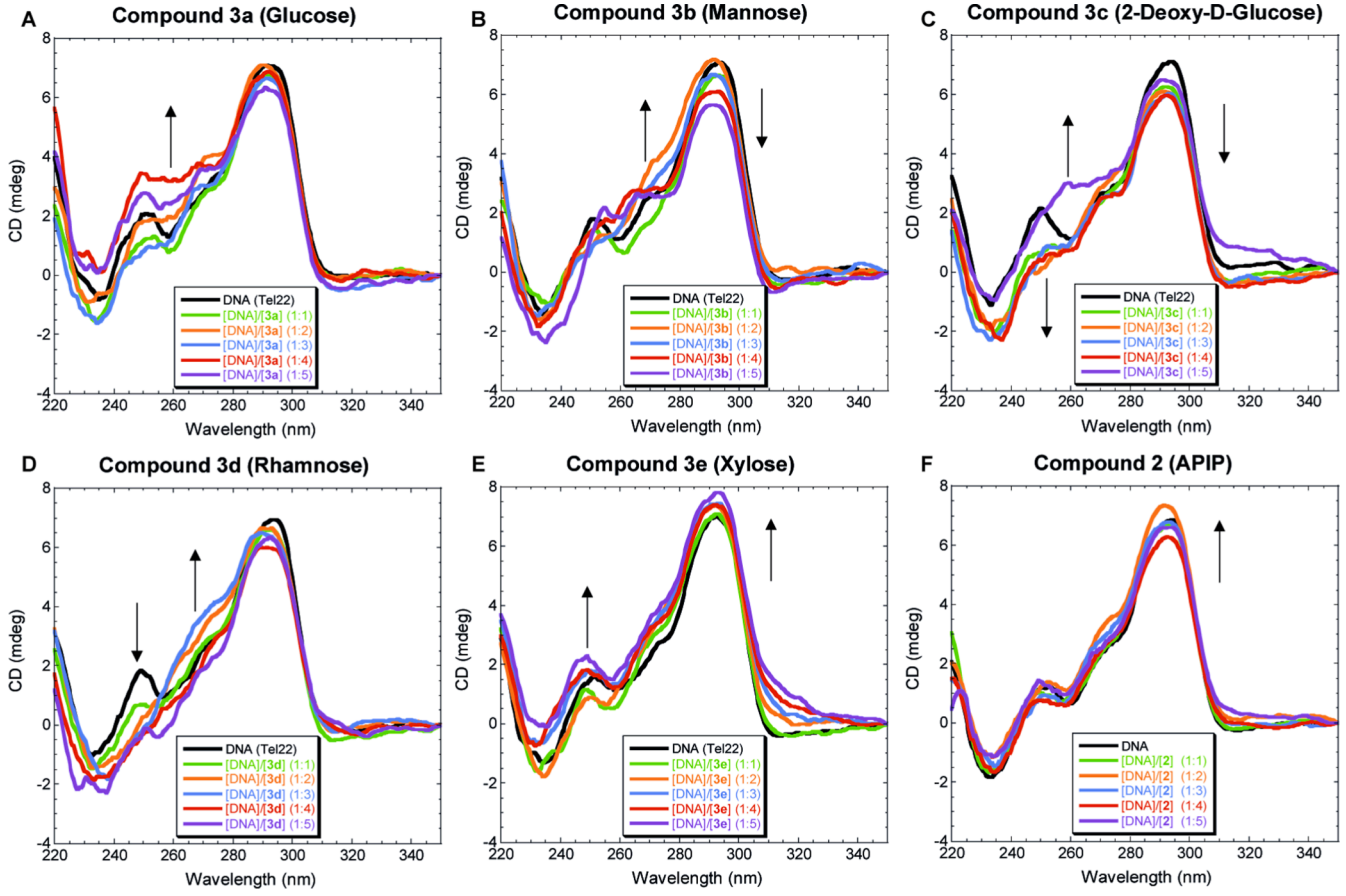

Fig. 3. Changes in CD spectra of quadruplex Tel22 (4 μM strand molarity), folded in the presence of potassium ions, (10 mM lithium cacodylate, 90 mM LiCl, 10 mM KCl, pH 7.3, 25 °C) upon addition compounds **3a-e** and **2** in a molar ratio DNA/Compound ranging from 1:1 to 1:5. A) Tel22 + **3a**. B) Tel22 + **3b**. C) Tel22 + **3c**. D) Tel22 + **3d**. E) Tel22 + **3e**. F) Tel22 + **2**.

slight stabilization of the telomeric hybrid-type topology, as revealed by the increase in intensity of the characteristic spectral bands.

Finally, it is important to point out that the effects observed in the CD spectra are a consequence of the presence of the carbohydrate moiety, because the precursor compound, amine **2**, under the same experimental conditions, did not show alteration on the CD spectral signature of Tel22, beyond a slight ellipticity enhancement at 295 nm (Fig. 3F).

Taken together, the experiments revealed that the carb-APIPs under investigation can induce appreciable modifications on the CD spectrum of Tel22 and confirm their binding to this particular secondary structure. Furthermore, our results suggest that the spectral changes observed are not totally uniform, as they are dependent on the particular carbohydrate, in good agreement with previous work with other carbohydrate analogues [15b].

2.2.3. Equilibrium dialysis

Equilibrium dialysis experiments with the quadruplex telomeric sequence Tel22 were carried out to determine apparent binding association constants. The experiments were adapted from the technique developed by the Chaires group [27], which is based on the fundamental thermodynamic principle of equilibrium dialysis [28] and the Crothers competition dialysis method [29].

2 μM solutions of compounds **3a-e** (dialysate solutions, 100 mM KCl) were equilibrated with 75 μM of nucleic acid for 24 h. (Under these conditions, compound **2** was found to precipitate in the buffer system and, therefore, it was not included in the study). At the end of the equilibration period, a detergent was added to the dialysis solutions, and UV–visible spectra were recorded in order to determine the concentrations of free and DNA-bound ligand. Apparent association constants were calculated by using the equation $K_{app} = C_b/(C_f)(S_{total}\text{-}C_b)$ [27c], where C_b is the amount of ligand bound, C_f is the free ligand concentration and $S_{total} = 75$ μM, in monomeric units (tetrads in this case).

Table 3 shows that compounds **3a-e** have a good affinity for telomeric G-quadruplex DNA, with apparent association constants in the order of 10^5 M^{-1}. In general, these derivatives show a similar grade of affinity towards the quadruplex structure, although dependent of the type of carbohydrate. This behavior resembles that previously observed with the family of the copper(II)complexes of *N*-(1,10-phenanthrolin-5-yl)-β-glycopyranosylamines. Under the present conditions, the 2-deoxyglucose (**3c**) and rhamnose (**3d**) derivatives exhibited the highest binding affinity, closely followed by the glucose-APIP **3a**. On the other hand, the mannose (**3b**) and xylose (**3e**) compounds presented the lowest K_{app} values. However, it is important to highlight that the association constants determined for the carb-APIPs alone, possessing an extended aromatic surface, were found to be one order of magnitude higher than those obtained in the case of two molecules of *N*-(1,10-phenanthrolin-5-yl)-β-glycopyranosylamine coordinated to Cu(II).

Additional dialysis experiments with *Calf Thymus* (CT) dsDNA were carried out. In general, even if the experimental conditions (such as ionic strength, biomolecule size and sequence) are not exactly comparable, it was found that apparent binding constant values were lower than those determined with telomeric quadruplex structures, except for compound **3e**. Interestingly, compounds **3c** and **3d** revealed a binding affinity to dsDNA ~ 6-fold and ~ 13-fold lower than to G4 Tel22, respectively. The xylose derivative **3e**, on the other hand, and in the experimental conditions tested, showed a remarkable affinity towards dsDNA, higher than **3a** and **3b**, and much higher than **3c** and, especially, than **3d** (2-deoxyglucose and rhamnose derivatives, respectively). This finding points towards the fact that the rhamnose- and 2-deoxyglucose-APIPs can be considered the best quadruplex ligands in terms of binding affinity to the target quadruplex sequence.

2.2.4. Viscosity assays

As the preceding interaction studies performed on carb-APIPs **3a-e** revealed that the compounds bind the telomeric quadruplex efficiently, but they can as well recognize dsDNA, we settled out to investigate the mode of interaction with the latter. This can be approached by using a relatively simple assay, viscosity titrations, which allow determining whether a compound of interest binds duplex DNA either by intercalation between the DNA base pairs, which results in an increase of the solution viscosity, or by binding to the DNA grooves, or externally [30], which barely affects its viscosity. For that purpose, the theory of Cohen and Eisenberg was applied [31], and gradual titrations of DNA solutions with the carb-APIPs were carried out. This produced linear plots of the cubed root of the relative DNA viscosity $(\eta/\eta_o)^{1/3}$ versus the molar ratio of bound ligand to DNA nucleotide (r), from which slope values were determined. These values can be roughly correlated with DNA-ligand binding modes in the following way: groove binding compounds commonly display a slope close to 0.0, whereas classical intercalating molecules, such as ethidium bromide (monointercalant) give rise to slope values close to 1.0 [30,31]. Experimentally, it has been found that the slopes associated with minor-groove binder compounds can vary within the range from −0.3 to 0.2 [32].

Viscometric assays were carried out at a temperature of 25 ± 0.01 °C by adding small aliquots of each carb-APIP **3a-e** (or compound **2** or selected controls) to the DNA solutions of *Calf Thymus* (CT) DNA, in 10 mM sodium phosphate buffer (pH 7.2). Flow times were recorded in the presence (η) and in the absence (η_o) of compound. The viscosity data were plotted as $(\eta/\eta_o)^{1/3}$ versus r, as shown in Fig. 4.

Compounds **3a-e** demonstrated a linear $(\eta/\eta o)^{1/3}$ versus r correlation at the ligand to DNA molar ratios used in the experiments. The compound slope values resulting from the viscosity plots ranged from 0.23 (**3d**) to 0.46 (**3b**). The mannose derivative **3b**, which displayed the lowest quadruplex selectivity in FRET melting assays gave rise to the highest slope in the dsDNA viscosity titration. On the contrary, the rhamnose derivative **3d**, which displayed high affinity and selectivity for the telomeric quadruplex in the preceding experiments, yielded the lowest slope value. **3a** and **3e** showed almost identical behavior with a slope value ~ 0.30 and, to a lesser extent, **3b** and **3c**, with values of ~ 0.47 and ~ 0.40, respectively (Fig. 4). Compound **2**, the precursor amine, gave rise to a slope value similar to the mannose (**3b**) and 2-deoxyglucose (**3c**) derivatives, ~ 0.44.

It is evident from the results obtained that these carb-APIPs do not interact with dsDNA by a classical intercalation mechanism, but rather by a mixed binding mode involving groove binding and, in some cases, partial or not classical intercalation. The rhamnose derivative **3d** is likely to bind the DNA grooves or externally, while the mannose derivative **3b** stands out in the carb-APIP series for a higher contribution of intercalation, although this cannot be considered a classical intercalator, such as ethidium bromide (Fig. 4, slope ~ 1.02). Notwithstanding, it is important to remark that the differences in the viscosity slope values are not sufficient to account for significant differences in binding modes, and they suggest that these carb-APIPS and the precursor compound **2** interact with duplex DNA in a similar fashion, with a highest, but modest

Table 3
Apparent association constants for carb-APIPs **3a-e** obtained by equilibrium dialysis.

	3a (Glucose)	**3b (Mannose)**	**3c (2-Deoxyglucose)**	**3d (Rhamnose)**	**3e (Xylose)**
DNA	K_{app} (M^{-1}) × 10^{-5}	K_{app} × 10^{-5}	K_{app} × 10^{-5}	K_{app} × 10^{-5}	K_{app} × 10^{-5}
Tel22 (G-quadruplex, K^+)	3.15 ± 0.08	2.02 ± 0.18	4.18 ± 0.01	3.70 ± 0.30	1.06 ± 0.03
CT dsDNA (no salt)	2.32 ± 0.56	1.15 ± 0.30	0.71 ± 0.01	0.29 ± 0.01	5.20 ± 0.13

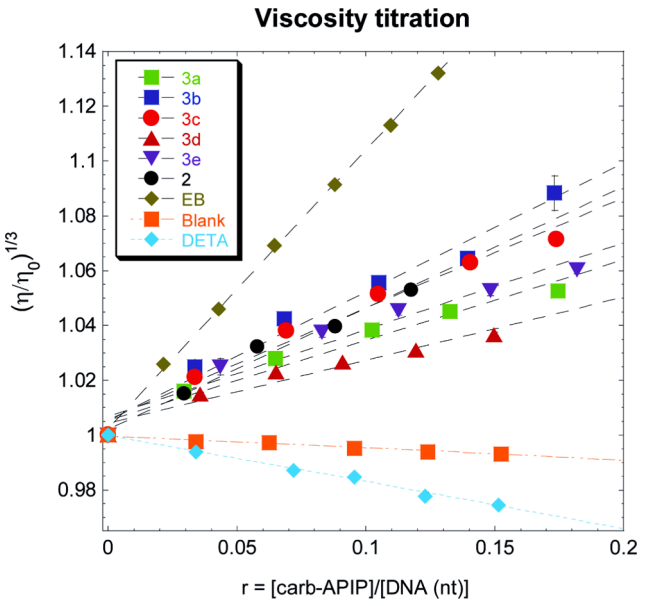

Fig. 4. Viscosity titration experiments of *Calf Thymus* (CT) DNA and carb-APIPs **3a-e** at 25 °C (10 mM sodium phosphate buffer, pH 7.2). Averaged slope values are, ca.: 0.29 **(3a)**, 0.47 **(3b)**, 0.40 **(3c)**, 0.23 **(3d)**, 0.31 **(3e)**, 0.44 **(2)**, 1.02 **(EB)**, −0.04 (blank, no compound), −0.17 **(DETA)**. EB: *ethidium bromide (classical intercalant);* DETA*: diethylenetriamine (non-specific, electrostatic binder).*

contribution of intercalation in the case of compounds **3b**, **2** and **3c**, and a higher contribution of groove binding for the rhamnose derivative **3d**.

Although these finding cannot be directly extrapolated to quadruplex DNA, which differs in the number and dimensions of the grooves and it presents a highly dynamic character, these results allow us to hypothesize that **3a-e** interact with the human telomeric quadruplex, besides by π-π stacking interactions, by recognizing the grooves and/or loops of the structure, likely establishing hydrogen-bond interaction networks between the carbohydrate and the phosphate backbones.

2.3. Cytotoxic activity in cultured cells

Finally, we tested the biological antitumor activity of carb-APIPs in cultured PC3 (prostate), HeLa (cervix) and MCF7 (breast) cancer cells and in normal human fibroblast (HFF1) cells, by the MTT assay, after a 72 h treatment. In addition, effects on cell cycle progression were studied preliminarily. G-quadruplex ligand 360A and cisplatin were included in some of the experiments for comparison purposes, as they are known cytotoxic compounds, as well as the carb-APIP amine precursor, compound **2**. In addition, the cytotoxicity in cancer cells of some representative derivatives (**4**–**7**) of the *N*-(1,10-phenanthrolin-5-yl)-β-glycopyranosylamines series is also reported in this work (Table S2) to compare the two families of derivatives, and to establish whether an increase in aromatic surface is exerting an effect on antitumor activity. Other carbohydrate analogues, the N^1-(4,5-diazafluoren-9-yliden)–N^2-glycopyranosyl hydrazines, have been previously found inactive up to a 100 μM concentration [15c].

The results from this assay revealed that most of the compounds, after a 72 h treatment, have significant antitumor activity in cultured cells, as they are cytotoxic in the low micromolar concentration range, with IC_{50} values around 10 μM and below (Table 4, Figures S24-S26) in HeLa and PC3 cell lines, and slightly higher (up to 34 μM) in MCF7. Their antitumor activity is comparable to that determined for the quadruplex ligand 360 and significantly higher than the metallo-drug cisplatin. As a matter of fact, all carb-APIPs exhibited a better antitumor activity than the reference compounds in the MCF7 breast cancer cell line. Although their relative antitumor activity is similar and dependent on the cell line tested, in general, 2-deoxyglucose-APIP (**3c**) demonstrated the higher antitumor activity in the series, followed by the rhamnose and the xylose-APIPs (**3d** and **3e**), then the mannose (**3b**) and, finally, by the glucose (**3a**) derivative. Compound **2** showed a significant cytotoxicity activity as well, especially relevant in the MCF7 cell line, with IC_{50} values in the range 4–6 μM. MTT assays performed with the previously reported *N*-(1,10-phenanthrolin-5-yl)-β-glycopyranosylamines (Table S2), revealed that all carb-APIPs reported in this work have better antitumor biological activity (lower IC_{50} values), suggesting that an increased aromatic surface and the particular structural features of the carb-APIPs are clearly beneficial.

Table 4
Cytotoxic activity of compounds **3a-e, 2** and selected controls in tumor PC3, HeLa, and MCF7 cultured cells and normal fibroblast (HFF1) cells after 72 h incubation.[a]

	PC3	Hela	MCF7	HFF1	SI[b,c]
Compound	IC_{50} (μM)	IC_{50} (μM)	IC_{50} (μM)	IC_{50} (μM)	
2	4.3 ± 0.9	6.1 ± 2.3	5.2 ± 1.0	15.8 ± 0.8	3.7[b] 3.0[c]
3a (glucose)	8.3 ± 2.3	7.9 ± 1.5	33.5 ± 3.1	33.2 ± 5.0	4.0[b] 1.0[c]
3b (mannose)	4.3 ± 1.3	6.7 ± 1.4	21.5 ± 1.4	26.4 ± 2.5	6.1[b] 1.2[c]
3c (2-deoxyglucose)	1.9 ± 0.6	5.5 ± 0.8	7.9 ± 0.4	10.5 ± 1.8	5.5[b] 1.3[c]
3d (rhamnose)	4.4 ± 0.4	4.7 ± 1.3	22.9 ± 1.3	40.0 ± 6.8	9.1[b] 1.7[c]
3e (xylose)	3.9 ± 0.8	10.9 ± 2.6	14.7 ± 2.3	21.2 ± 2.9	5.4[b] 1.4[c]
360A	2.5 ± 0.8	8.5 ± 1.4	44.9 ± 9.2	30.6 ± 2.3	12.2[b]0.7[c]
Cisplatin	12.8 ± 0.9	18.0 ± 1.9	96.5 ± 6.7	36.4 ± 4.4	2.8[b] 0.4[c]

[a] IC_{50} values for reference compounds 360A and cisplatin were determined under identical experimental conditions [33].
[b] SI (Safety or selectivity index) determined as IC_{50} (HFF1)/IC_{50} (PC3).
[c] SI determined as IC_{50} (HFF1)/IC_{50} (MCF7).

Regarding the carb-APIPs cytotoxicity in normal cells, a preliminary study with human fibroblasts (HFF1 cell line, Table 4, Figure S27) indicates that the carb-APIPs, compound **2**, and reference antitumor compounds (360A and cisplatin) are moderately less cytotoxic in the healthy cells, especially in comparison with cytoxicity results obtained in PC3 and Hela cells. The selectivity indexes (SI), determined with respect to PC3 cells, for example, reflect selectivities for the carb-APIPs in the range 4 to 9-fold, higher than cisplatin, but lower than compound 360A. The best compound in the carb-APIP series turned out to be **3d**, the rhamnose derivative, with an estimated 9-fold selectivity. The selectivity effect is considerably diminished when referred to MCF7 cells, in particular for the antitumor reference compounds, 360A and cisplatin. Even in this case, the family of carb-APIPs shows more selectivity than the controls, with exception made for compound **2**, which possesses a remarkable cytotoxic antitumor activity in MCF7.

Finally, preliminary cell cycle arrest assays using flow cytometry were carried out, in HeLa cells, treated with the compounds at IC_{50} equivalent concentrations, for 72 h. Under these conditions (5 and 10 μM of carb-APIP) modest alterations in the cell cycle distribution (SubG0, G0/G1, S or G2/M populations) were detected. After 72 h of incubation, it was found that most of the carb-APIPs arrested cell cycle at the G0/G1 phase (Figure S29, 10 μM concentration, ~ 5–7% increase relative to control), whereas the amine precursor, compound **2**, and **3d** (rhamnose derivative), minimally affected this cell phase. Compounds **3b**, **3c**, **3e** and **2** produced a similar decrease in the number of cells in S and G2/M (~7–9%) phases and a slight increase of SubG0 (~2–3%), the population of apoptotic cells, whereas **3d** showed a distinctive increase of the number of cells in S phase (~5%) and subsequent decrease in G2/M. Additional experiments testing the rhamnose derivative, compound **3d**, along with 360A, cisplatin and **2**, in HeLa cells (Figure S30) confirmed that **3d** exerts minor effects on HeLa cell cycle progression compared to the antitumor reference ligands used in the present study, interfering with DNA synthesis. However, the distinctive effects observed among the different carb-APIPs and between this family of compounds and precursor **2**, once again highlight the important role that the carbohydrate subunit must play to confer the carb-APIP conjugates with the particular biological properties. Further investigation

under a wider range of experimental conditions with a panel of different cell lines will be needed to fully characterize the effects of the compounds on cancer cell cycle progression.

3. Conclusions

Treatment of 2-(4-aminophenyl)-1*H*-imidazo[4,5-f][1,10]phenanthroline with different unprotected monosaccharides afforded a novel series of *N*-4-(1*H*-imidazo[4,5-f][1,10]phenanthrolin-2-yl)phenyl-β-glycopyranosylamines (carb-APIPs) with synthetically useful yields and excellent stereoselectivity. Interestingly, these carbohydrate conjugates underwent in solution a dynamic equilibrium leading to anomeric mixtures with small participation of the α isomer.

In addition, we have reported the interactions of the novel carb-APIPs **3a-e** with the human telomeric quadruplex sequence, folded in the presence of potassium ions. This family of compounds has shown a significant ability to bind telomeric G-quadruplex DNA, as established by FRET-based DNA melting experiments, in non-competitive and in a competitive version, by circular dichroism titrations, and by equilibrium dialysis. From the results obtained by competition FRET, it can be inferred that the presence of the carbohydrate is conferring quadruplex versus duplex DNA binding selectivity. In addition, the carb-APIPs are able to induce conformational changes in the telomeric structure that are dependent on the nature of the carbohydrate, as shown by CD titrations. All derivatives were found to bind quadruplex DNA with high affinity, determined by equilibrium dialysis experiments. Finally, additional viscosity experiments performed on dsDNA (CT) point towards an interaction that involves groove binding and, possibly, partial intercalation. The extended aromatic surface of these derivatives and structural characteristic of the compounds may not be optimal for binding to dsDNA by classical intercalation. Therefore, the results described herein are consistent with a DNA-ligand interaction that may involve, at least in part, the recognition of the DNA grooves and/or loops of the telomeric quadruplex besides the typical π-π stacking interactions with the external tetrads of the G-quadruplex. This groove binding is likely to be conditioned by the nature of the particular carbohydrate component of each carb-APIP.

Regarding the biological activity, all derivatives have shown significant antitumor activity in HeLa, PC3 and MCF7 tumor cell lines, with IC_{50} values in the low micromolar concentration range. At the same time, they also have proven cytotoxic in normal fibroblast cells (HFF1), although to a lower extent that in PC3 and HeLa cells, which confers the compounds with modest but interesting selectivity, especially in the case of the rhamnose derivative **3d**. Their antitumor activity and selectivity compare well with that observed for quadruplex ligand 360A and they are significantly better than cisplatin metallo-drug, especially in the breast cancer cell line (MCF7). Moreover, compared to other carbohydrate derivatives reported previously [15b,15c], the conjugation with the 2-(4-aminophenyl)-1*H*-imidazo[4,5-f][1,10]phenanthroline core (APIP) confers the compounds with an increased biological activity, without the need of further coordination to a metal species. Finally, preliminary cell cycle assays suggest that the carbohydrate conjugates, at IC_{50} equivalent concentrations, modestly affect cell cycle progression in HeLa cells, resulting in a slight increase in the G0/G1 and SubG0 populations. In addition, the rhamnose derivative **3d** seems to promote cell cycle arrest in S phase. Further studies with selected candidates will be required to shed more light on the underlying mechanisms that account for the biological activity of the carb-APIPs.

4. Experimental

4.1. General methods

All reagents were commercially available (Sigma-Aldrich) in high purity and used as received. The *N*-glycosylation reactions were monitored by thin-layer chromatography (TLC) and their composition was determined by ^{1}H NMR spectroscopy; TLC was performed on precoated Kieselgel 60 F_{254} aluminum sheets; plates were eluted with methanol, dried and then eluted with methanol/ NH_4OH (30%) 10:0.7; detection was first by UV and then by charring with sulphuric acid in ethanol (1:4, v/v). Melting points were taken on an Electrothermal Digital IA9100 apparatus and were uncorrected. Optical rotations were measured in HPLC grade dimethylsulfoxide on a Perkin-Elmer 341 polarimeter; $[\alpha]_D$ values are given in 10^{-1} deg•cm^2•g^{-1}; concentration is given in mg•mL^{-1}. ESI mass (+mode) spectra were performed on a Thermo Scientific TSQ Quantum LC/MS or an AB Sciex QSTAR Pulsar Q-TOF instruments. IR spectra (KBr disks) were recorded on a FT-IR Perkin-Elmer Spectrum 2000 spectrophotometer. All NMR spectra (^{1}H, ^{13}C, 2D ^{1}H–^{1}H gCOSY, TOCSY, ROESYAD, ^{1}H–^{13}C gC2HSQCSE, gHMBC) were recorded on a Varian 300 UNITY-Plus or VNMRS-500 and Brucker-400 spectrometers in $(CD_3)_2SO$ or $(CD_3)_2SO/D_2O$ at 298 K using standard pulse sequences. Chemical shifts are reported relative to the residual $(CHD_2)_2SO$ (δ_H 2.50 ppm), or $(CD_3)_2SO$ (δ_C 39.5 ppm); resonance patterns are designated with the notations s (singlet), d (doublet), t (triplet), q (quartet), and m (multiplet); in addition, the notations ap and br are used to indicate an apparent multiplicity and a broad signal; geminal H-6′ protons at the sugar moieties resonating at low and high frequency are denoted as H-6′a and H-6′b, respectively; axial and equatorial protons of pyranose CH_2 groups are indicated as Hax and He. Lorentz-Gauss transformation was used to improve the resolution of the ^{1}H NMR spectra. Errors: ^{1}H, δ ± 0.01 ppm, J ± 0.1 Hz; ^{13}C, δ ± 0.1 ppm.

For DNA interaction studies, distilled, deionized water (ddH_2O, Milli-Q) was used for the preparation of all buffers and aqueous solutions. All reagents and solvents were synthesis or molecular biology grade and were utilized as provided by Sigma-Aldrich. Carb-APIPs solutions were freshly prepared for each assay, including a small percentage of DMSO as co-solvent in the concentrated solutions, from which working solutions in water were made by serial dilution.

4.2. Synthesis of 2-(4-Aminophenyl)-1H-imidazo[4,5-f][1,10] phenanthroline (2)

2-(4-Aminophenyl)-1*H*-imidazo[4,5-f][1,10]phenanthroline (**2**) was prepared in two steps from 1,10-phenanthroline-5,6-dione [34] as previously described [4c,6o,35] with small variations. Firstly, treatment of the 1,10-phenanthroline-5,6-dione with 4-nitrobenzaldehyde and NH_4OAc (molar ratio dione/aldehyde/NH_4OAc 1:1.2:20) in glacial HOAc ([dione] = 0.1 M) at 124 °C for 5 h led to 2-(4-nitrophenyl)-1*H*-imidazo[4,5-f][1,10]phenanthroline [4c,35] with a yield of 94%. Reduction of nitro derivative with hydrazine hydrate using Pd/C 10% as catalyst [6o] at 70 °C for 6 h afforded **2** as a dark orange powder (97%). δ_H (300 MHz; $(CD_3)_2SO$) 5.64 (2H, br s, NH_2), 6.74 (2H, dap, J = 8.7 Hz, H-3′(5′)), 7.81 (2H, dd, J = 8.1, 4.3 Hz, H-5(10)), 7.97 (2H, dap, J = 8.7 Hz, H-2′(6′)), 8.90 (2H, dd, J = 8.1, 1.8 Hz, H-4(11)), 9.00 (2H, dd, J = 4.3, 1.8 Hz, H-6(9)), 13.30 (1H, s, NH); δ_C (75 MHz; $(CD_3)_2SO$) 113.6 (C-3′(5′)), 117.3 (C-1′), 123.2 (C-5(10)), 125.5[a] (C-3b(11a)), 127.6 (C-2′(6′)), 129.4 (C-4(11)), 135.4[a] (C-3a(11b)), 143.2 (C-7a(7b)), 147.4 (C-6(9)), 150.5 (C-2), 152.1, (C-4′); [a] values deduced from ^{1}H–^{13}C gHMBC spectrum, tentative assignment.

4.3. Synthesis of N-4-(1H-imidazo[4,5-f][1,10]phenanthrolin-2-yl) phenyl-β-glycopyranosylamines general procedure

To a stirred solution of the 2-(4-aminophenyl)-1*H*-imidazo[4,5-f][1,10]phenanthroline (156 mg, 0.5 mmol) in 10 mL of methanol ([amine] = 0.05 M) was added the monosaccharide (1.5 mmol) and ca. 4 mg of $(NH_4)_2SO_4$ [15a]. The reaction mixture was heated at 60 °C for 24 h and then allowed to cool to room temperature. The solid obtained was separated by filtration and washed with MeOH (2 × 10 mL) and H_2O (2 × 10 mL) to remove the $(NH_4)_2SO_4$ salt and to eliminate excess of sugar as well as possible traces of the starting amine and/or other by-products, and then treated with Et_2O. After drying in vacuum, the

purity of the *N*-glycopyranosylamines **3a-e** was checked by TLC, ^{1}H NMR and analytical data.

***N*-4-(1H-imidazo [4,5-f] [1,10] phenanthrolin-2-yl)phenyl-β-*D*-glucopyranosylamine (3a).** White solid; yield: 78%; R_f = 0.42; mp 245–247 °C (decomposition); $[\alpha]_D^{22}$ −21 (*c* 1.11 in DMSO); IR (KBr) ν_{max} 3292 br (NH and OH), 1614 (δ NH), 1566, 1529, 1483 (C═N, C═C), 1077, 1022 cm^{-1}; δ_H (500 MHz; $(CD_3)_2SO$) 3.15 (1H, tdap, *J* = 9.5, 9.2, 5.1 Hz, H-4), 3.22 (1H, tdap, *J* = 8.9, 8.6, 5.5 Hz, H-2), 3.29[a] (2H, m, H-3, H-5), 3.47 (1H, dtap, *J* = -11.9, 6.1,5.8 Hz, H-6a), 3.70 (1H, ddd, *J* = −11.9, 5.5, 2.1 Hz, H-6b), 4.48 (1H, tap, *J* = 5.8, 5.5 Hz, OH-6), 4.50 (1H, tap, *J* = 8.6, 7.6 Hz, H-1), 4.93[b] (1H, d, *J* = 5.5 Hz, OH-2), 4.93[b] (1H, d, *J* = 5.1 Hz, OH-4), 5.01 (1H, d, *J* = 4.6 Hz, OH-3), 6.77 (1H, d, *J* = 7.6 Hz, NH), 6.90 (2H, dap, *J* = 8.9 Hz, H-2′(6′)), 7.80 (1H, dd, *J* = 8.0, 4.2 Hz, H-5″(10″)), 7.84 (1H. dd, *J* = 8.2, 4.2 Hz, H-5″(10″)), 8.05 (2H, dap, *J* = 8.9 Hz, H-3′(5′)), 8.90[c] (1H, dd, *J* = 8.0, 1.8 Hz, H-4″(11″)), 8.90[c] (1H, dd, *J* = 8.2, 1.8 Hz, H-4″(11″)), 9.01[d] (1H, dd. *J* = 4.2, 1.8 Hz, H-6″(9″)), 9.02[d] (1H, dd, *J* = 4.2, 1.8 Hz, H-6″(9″)), 13.38 (1H, s, NH-1″); δ_C (125 MHz; $(CD_3)_2SO$) 60.9 (C-6), 70.2 (C-4), 73.0 (C-2), 77.5, 77.8 (C-3, C-5), 84.4 (C-1 $^1J_{C1\text{-}H1}$ = 150 Hz), 113.2 (C-2′(6′), 118.7, 119.3 (C-4′, C-3″b(11a″)), 123.0, 123.2 (C-5″(10″)), 125.8[e] (C-3″b (11″a)), 127.3 (C-3′(5′)), 129.3, 129.5 (C-4″(11″)), 135.7[e] (C-3a"(11″b)), 143.0, 143.5[e] (C-7″a(7″b)), 147.3, 147.5 (C-6″(9″), 148.8 (C-1′), 151.7 (C-2″); [a] 3.30 (1H, tap, *J* = 8.9, 8.8 Hz, H-3), 3.30 (1H, m, H-5) partially overlapped signals in $(CD_3)_2SO$-D_2O; [b,c,d] overlapped signals; [e] values corroborated from ^{1}H–^{13}C gHMBC spectrum, tentative assignment. HRMS (ESI-TOF): $(M+H)^+$, found 474.1776 $C_{25}H_{24}N_5O_4$ requires 474.1772. When the NMR spectra were registered after 24 h some signals corresponding to α anomer were also identified, δ $_H$ (500 MHz; $(CD_3)_2SO$-D_2O): 5.02 (1H, d, *J* = 4.9 Hz, H-1), 7.10 (2H, dap, *J* = 8.8 Hz, H-2′(6′)).

***N*-4-(1H-imidazo [4,5-f] [1,10] phenanthrolin-2-yl)phenyl-β-*D*-mannopyranosylamine (3b).** White powder; yield: 79%; R_f = 0.41; mp 203–205 °C (decomposition); [Found: C, 60.98; H, 4.91; N, 13.98. $C_{25}H_{23}N_5O_5{\cdot}H_2O$ requires C, 61.09; H, 5.13; N, 14.25%]; $[\alpha]_D^{22}$ −85 (*c* 1.64 in DMSO); IR (KBr) ν_{max} 3369 br (NH and OH), 1615 (δ NH), 1528, 1484 (C═N, C═C), 1074 cm^{-1}; δ_H (500 MHz; $(CD_3)_2SO$) 3.24 (1H, ddd, *J* = 9.2, 6.1, 2.1, H-5), 3.41 (1H, tdap, *J* = 9.4, 9.2, 5.2 Hz, H-4), 3.46[a] (1H, ddd, *J* = 9.4, 5.7, 3.8 Hz, H-3), 3.47[a] (1H, dt, *J* = -11.6, 6.1 Hz, H-6a), 3.70 (1H, ddd, *J* = -11.6, 5.5, 2.1 Hz, H-6b), 3.79 (1H, br tap, *J* = 5.2, 3.8H, H-2), 4.39 (1H, tap, *J* = 6.1, 5.5 Hz, OH-6), 4.77[b] (1H, d, *J* = 5.2 Hz, OH-4), 4.78[b] (1H, d, *J* = 5.7 Hz, OH-3), 4.82 (1H, d, *J* = 5.2 Hz, OH-2), 4.87 (1H, dap, *J* = 9.5 Hz, H-1), 6.31 (1H, d, *J* = 9.5 Hz, NH), 6.97 (2H, dap, *J* = 8.9 Hz, H-2′(6′)), 7.80 (1H, dd, *J* = 8.2, 4.3 Hz, H-5″(10″)), 7.84 (1H. dd, *J* = 8.2, 4.3 Hz, H-5″(10″)), 8.04 (2H, dap, *J* = 8.9 Hz, H-3′(5′)), 8.90[c] (1H, dd, *J* = 8.2, 1.8 Hz, H-4″(11″)), 8.90[c] (1H, dd, *J* = 8.2, 1.8 Hz, H-4″(11″)), 9.01[d] (1H, dd. *J* = 4.3, 1.8 Hz, H-6″(9″)), 9.02[d] (1H, dd, *J* = 4.3, 1.8 Hz, H-6″(9″)), 13.38 (1H, s, NH-1″); δ_C (100 MHz; $(CD_3)_2SO$) 61.2 (C-6), 67.1 (C-4), 70.9 (C-2), 74.4 (C-3), 77.9 (C-5), 81.1 (C-1 $^1J_{C1\text{-}H1}$ = 150 Hz), 113.6 (C-2′(6′), 119.0, (C-4′, C-3″b (11a″)), 123.1 (C-5″(10″)), 125.6[e] (C-3″b(11″a)), 127.3 (C-3′(5′)), 129.4 (C-4″(11″)), 135.0[e] (C-3a″(11″b)), 143.2 (C-7″a(7″b)), 147.4 (C-6″(9″), 147.9 (C-1′), 151.7 (C-2″); [a,b,c,d] overlapped signals; [e] values deduced from ^{1}H–^{13}C gHMBC spectrum, tentative assignment. LRMS (ESI) *m/z* 474 $(M+H)^+$. When the NMR spectra were registered after 24 h some signals corresponding to α anomer were also identified, δ_H (500 MHz; $(CD_3)_2SO$): 6.85 (1H, d, *J* = 5.3 Hz, NH), 7.03 (2H, dap, *J* = 8.9 Hz, H-2′(6′)), 8.05 (2H, dap, *J* = 8.9 Hz, H-3′(5′)); δ_H (500 MHz; $(CD_3)_2SO$-D_2O): 4.97 (1H, d, *J* = 1.8 Hz, H-1).

***N*-4-(1H-imidazo [4,5-f] [1,10] phenanthrolin-2-yl)phenyl-β-2-deoxy-*D*-glucopyranosylamine (3c).** Beige solid; yield: 80%; R_f = 0.50; mp 233–235 °C (decomposition); $[\alpha]_D^{22}$ −60 (*c* 2.16 in DMSO); IR (KBr) ν_{max} 3309 br (NH and OH), 1614 (δ NH), 1566, 1529, 1484 (C═N, C═C), 1068 cm^{-1}; δ_H (500 MHz; $(CD_3)_2SO$) 1.60 (1H, cap, *J* = 11.6, −11.0, 10.7 Hz, H-2ax), 2.08 (1H, ddd, *J* = -11.0, 5.2, 1.5, H-2e), 3.06 (1H, tdap, *J* = 9.5, 8.8, 4.9 Hz, H-4), 3.24 (1H, ddd, *J* = 9.5, 5.8, 2.2 Hz, H-5), 3.49 (1H, dtap, *J* = -11.9, 5.8 Hz, H-6a) 3.54[a] (1H, m, H-3), 3.70 (1H, ddd, *J* = -11.9, 5.5, 2.2, H-6b), 4.43 (1H, tap, *J* = 5.8, 5.5 Hz, OH-6), 4.81 (1H, tdap, *J* = 10.7, 8.3, 1.5, H-1), 4.87 (1H, d, *J* = 5.2 Hz, OH-3), 4.90 (1H, d, *J* = 4.9 Hz, OH-4), 6.87 (2H, dap, *J* = 8.6 Hz, H-2′(6′)), 6.95 (1H, d, *J* = 8.3, NH), 7.80 (1H, dd, *J* = 8.0, 4.2 Hz, H-5″(10″)), 7.84 (1H. dd, *J* = 8.3, 4.2 Hz, H-5″(10″)), 8.04 (2H, dap, *J* = 8.6 Hz, H-3′(5′)), 8.89[b] (1H, dd, *J* = 8.0, 1.5 Hz, H-4″(11″)), 8.90[b] (1H, dd, *J* = 8.3, 1.5 Hz, H-4″(11″)), 9.01[c] (2H, br s, H-6″(9″)), 13.37 (1H, s, NH-1″); δ_C (100 MHz; $(CD_3)_2SO$) 37.2 (C-2), 61.1 (C-6), 71.5, 71.7 (C-3, C-4), 77,6 (C-5), 79.7 (C-1, $^1J_{C1\text{-}H1}$ = 150 Hz), 113.3 (C-2′(6′), 118.8, 119.2 (C-4′, C-3″b (11a″)), 123.0, 123.6 (C-5″(10″)), 125.7[d] (C-3″b(11″a)), 127.3 (C-3′ (5′)), 129.3 (C-4″(11″)), 135.6[d] (C-3a"(11″b)), 143.0, 143.4 (C-7″a (7″b)), 147.3 (C-6″(9″), 148.2 (C-1′), 151.7 (C-2″); [a] 3.55 (1H, ddd, *J* = 11.6, 8.5, 5.2 Hz in $(CD_3)_2SO$-D_2O; [b] overlapped signals; [c] 9.02 (2H, dd, *J* = 4.3, 1.8 Hz) in $(CD_3)_2SO$-D_2O;[d]tentative assignment. HRMS (ESI-TOF): $(M+H)^+$,found 458.1828 $C_{25}H_{24}N_5O_4$ requires 458.1823. When the NMR spectra were registered after 24 h some signals corresponding to α anomer were also identified, δ_H (500 MHz; $(CD_3)_2SO$): 1.72 (1H, tdap, *J* = −12.8, 11.6, 4.9 Hz, H-2ax), 2.02 (1H, br dd, *J* = −12.8, 5.2, Hz, H-2ec), 3.14 (1H, tap, *J* = 9.2, 8.8 Hz, H-4), 3.90 (1H, m, H-3), 4.30 (1H, sa, OH), 5.18 (1H, tap, *J* = 5.5, 4.9 Hz, H-1), 6.94 (1H, d, *J* = 5.5 Hz, NH), 7.02 (2H, dap, *J* = 8.9 Hz, H-2′(6′)); δ_C (100 MHz; $(CD_3)_2SO$) 78.4 (C-1, $^1J_{C1\text{-}1H}$ = 155 Hz).

***N*-4-(1H-imidazo [4,5-f] [1,10] phenanthrolin-2-yl)phenyl-β-*L*-rhamnopyranosylamine (3d).** Light orange solid; yield: 81%; R_f = 0.54; mp 218–220 °C (decomposition); $[\alpha]_D^{22}$ + 60 (*c* 2.13 in DMSO); IR (KBr) ν_{max} 3306 br (NH and OH), 1614 (δ NH), 1527, 1484 (C═N, C═C), 1073, 1057 cm^{-1}; δ_H (500 MHz; $(CD_3)_2SO$) 1.16 (3H, d, *J* = 6.1 Hz, CH_3-6), 3.19 (1H, tdap, *J* = 9.5, 9.2, 5.2 Hz, H-4), 3.31 (1H, dc, *J* = 9.2, 6.1 Hz, H-5), 3.41 (1H, ddd, *J* = 9.5, 5.5, 3.4 Hz, H-3), 3.78 (1H, br tap, *J* = 5.2, 3.4 Hz, H-2), 4.76 (1H, d, *J* = 5.5 Hz, OH-3), 4.80 (1H, d, *J* = 5.2 Hz, OH-4), 4.87 (1H, d, *J* = 9.5 Hz, H-1), 4.91 (1H, d, *J* = 5.2 Hz, OH-2), 6.23 (1H, d, *J* = 9.5 Hz, NH), 6.96 (2H, dap, *J* = 8.9 Hz, H-2′(6′)), 7.81 (1H, dd, *J* = 8.3, 4.2 Hz, H-5″(10″)), 7.85 (1H. dd, *J* = 8.3, 4.2 Hz, H-5″(10″)), 8.04 (2H, dap, *J* = 8.9 Hz, H-3′(5′)), 8.90 (2H, dd, *J* = 8.3, 1.8 Hz, H-4″(11″)), 9.01 (2H, dd, *J* = 4.3, 1.8 Hz, H-6″(9″)), 13.39 (1H, s, NH-1″); δ_C (100 MHz; $(CD_3)_2SO$) 18.1 (CH_3-6), 71.1 (C-2), 72.0 (C-4), 72.6 (C-5), 74.1 (C-3), 80.8 (C-1, $^1J_{C1\text{-}H1}$ = 150 Hz), 113.7 (C-2′(6′), 119.1, (C-4′, C-3″b(11a″)), 123.1, 123.3 (C-5″(10″)), 125.8[a] (C-3″b (11″a)), 127.4 (C-3′(5′)), 129.6 (C-4″(11″)), 135.7[a] (C-3a"(11″b)), 143.1, 143.4 (C-7″a (7″b)), 147.4, 147.5 (C-6″(9″), 147.9 (C-1′), 151.7 (C-2″); [a] tentative assignment. HRMS (ESI-TOF): $(M+H)^+$, found 458.1828 $C_{25}H_{24}N_5O_4$ requires 458.1823. When the NMR spectra were registered after 24 h some signals corresponding to α anomer were also identified, δ_H (500 MHz; $(CD_3)_2SO$): 1.12 (3H, d, *J* = 6.2 Hz, CH_3-6), 3.26 (1H, tdap, *J* = 9.2, 5.2 Hz, H-4), 3.72 (1H, ddd, *J* = 9.2, 6.1, 3.7 Hz, H-3), 3.81 (1H, tdap, *J* = 3.7, 1.5 Hz, H-2), 4.94 (1H, dd, *J* = 6.1, 1.5 Hz, H-1), 6.85 (1H, d, *J* = 6.1 Hz, NH), 6.98 (2H, dap, *J* = 8.8 Hz, H-2′(6′)), 8.05 (2H, dap, *J* = 8.8 Hz, H-3′(5′)); δ_C (100 MHz; $(CD_3)_2SO$) 70.7 (C-3), 83.2 (C-1, $^1J_{C1\text{-}1H}$ = 160 Hz), 113.3 (C-2′(6′).

***N*-4-(1H-imidazo [4,5-f] [1,10] phenanthrolin-2-yl)phenyl-β-*L*-xylopyranosylamine (3e).** Light orange solid; yield: 84%; R_f = 0.53; mp 178–180 °C (decomposition); $[\alpha]_D^{22}$ + 12 (*c* 2.41 in DMSO); IR (KBr) ν_{max} 3304 br (NH and OH), 1613 (δ NH), 1528, 1483 (C═N, C═C), 1049 cm^{-1}; δ_H (500 MHz; $(CD_3)_2SO$) 3.18–3.36[a] (4H, m, H-2, H-3, H4, H5ax), 3.70 (1H, dd, *J* = -10.9, 5.1 Hz, H-5e), 4.47 (1H, tap, *J* = 8.2, 8.0 Hz, H-1), 4.95 (1H, d, *J* = 5.2 Hz, OH), 4.99 (1H, d, *J* = 5.0 Hz, OH), 5.05 (1H, d, *J* = 4.3 Hz, OH), 6.75 (1H, d, *J* = 8.0 Hz, NH), 6.88 (2H, dap, *J* = 8.9 Hz, H-2′(6′)), 7.80 (1H, dd, *J* = 8.0, 4.3 Hz, H-5″(10″)), 7.84 (1H. dd, *J* = 8.0, 4.3 Hz, H-5″(10″)), 8.05 (2H, dap, *J* = 8.9 Hz, H-3′(5′)), 8.90[b] (1H, dd, *J* = 8.0, 1.8 Hz, H-4″(11″)), 8.92[b] (1H, dd, *J* = 8.0, 1.8 Hz, H-4″(11″)), 9.01[c] (1H, dd, *J* = 4.3, 1.8 Hz, H-6″(9″)), 9.02[c] (1H, dd, *J* = 4.3, 1.8 Hz, H-6″(9″)), 13.38 (1H, s, NH-1″); δ_C (100 MHz; $(CD_3)_2SO$) 66.4 (C-5), 69.8 (C-4), 72.9 (C-2), 77.6 (C-3), 85.0 (C-1, $^1J_{C1\text{-}H1}$ = 150 Hz), 113.1 (C-2′(6′), 118.7, (C-4′, C-3″b(11a″)), 123.0 (C-5″(10″)), 125.6[d] (C-3″b(11″a)), 127.2 (C-3′(5′)), 129.3 (C-4″(11″)), 135.5[d] (C-3a"(11″b)), 142.9, 143.2 (C-7″a (7″b)), 147.2 (C-6″(9″), 148.5 (C-1′), 151.5 (C-2″);

[a]3.20 (1H, tap, J = 8.6 Hz, H-2), 3.25[e] (1H, tap, J = -11.0, 10.4 Hz, H-5ax), 3.25[e] (1H, tap, J = 8.6 Hz, H-3), 3.34 (1H, ddd, J = 10.4, 8.6, 5.2 Hz, H-4) in $(CD_3)_2SO$-D_2O; [b,c,e] overlapped signals; [d] tentative assignment. HRMS (ESI-TOF): $(M+H)^+$, found 444.1663 $C_{24}H_{22}N_5O_4$ requires 444.1666. When the NMR spectra were registered after 24 h some signals corresponding to α anomer were also identified, δ_H (500 MHz; $(CD_3)_2SO$): 6.46 (1H, d, J = 6.5 Hz, NH); δ_H (500 MHz; $(CD_3)_2SO$-D_2O): 5.00 (1H, d, J = 4.0 Hz, H-1); δ_C (100 MHz; $(CD_3)_2SO$) 80.7 (C-1, $^1J_{C1\text{-}1H}$ = 155 Hz).

4.4. DNA FRET melting assays

DNA FRET melting experiments were run according to previously reported protocols [33]. Labeled oligonucleotides F21T (5′- FAM – (GGG TTA)$_3$GGG – TAMRA – 3′) and F10T (5′- FAM – TAT AGC TA TA/Sp18/ TA GCT ATA – TAMRA – 3′) were dissolved in BPC grade water to provide 50 μM stock solutions. 0.25 μM solutions of F21T and F10T were then prepared by mixing the DNA stock solution (50 μM), the corresponding 2X buffer (K^+ salt) and water. These solutions were heated at 90 °C for 5 min and then cooled at 0 °C (F21T) or gradually to room temperature (F10T) for three hours. The solutions were allowed to stand overnight at 4 °C.

Compounds **3a-3e** were dissolved in water, containing a small proportion of DMSO (25 μM stock solution, DMSO % < 0.04 %). Carb-APIPs were tested at a concentration range from 0 to 5 μM using the oligonucleotide sequences F21T and F10T. Each well of the 96-well microplate contained a 50 μL total volume with a 200 nM oligonucleotide concentration in the corresponding buffer pH = 7.3. The buffering system for F21T contained 10 mM potassium chloride, 90 mM lithium chloride and 10 mM lithium cacodylate; the buffer used with F10T contained 100 mM lithium chloride and 10 mM lithium cacodylate.

The experiments were performed on an ABI PRISM® 7000 Sequence Detection System (Applied Biosystems). The melting procedure included a 5-min incubation at 24 °C followed by a temperature ramp at a 1 °C/min rate with fluorescence measurement at every degree up to 95 °C. The melting curves were obtained as a change in emission of FAM (6-carboxyfluorescein) excited at 492 nm and emitting at 516 nm. Experiments were run at least in duplicate. The melting temperatures (T_m) were determined from normalized curves as the mid-transition $T_{1/2}$ temperatures. $T_{1/2}$ represents an apparent melting temperature, defined as the temperature where the normalized fluorescence has a value of 0.5.

The competition FRET melting assays were carried out by employing analogous experimental conditions and following the same protocol as the non-competition experiments, with the F21T sequence and a carb-APIP concentration of 5 μM, in the absence or in the presence of DNA duplex competitor sequence ds26 (5′-CAA TCG GAT CGA ATT CGA TCC GAT TG-3′). Experiments were run in triplicate. Two different dsDNA concentrations were tested: 3 μM (15-fold duplex excess) and 10 μM (50-fold duplex excess). Selectivity of quadruplex versus duplex binding (S) was calculated at the two dsDNA tested concentrations according to the formula $S = (\Delta T_m)_{\text{with dsDNA competitor}}/(\Delta T_m)_{\text{without dsDNA competitor}}$.

4.5. Circular dichroism

Experiments were performed as previously reported [33]. The CD spectra were obtained using a Jasco J-715 spectropolarimeter. CD experiments were carried out with the DNA oligonucleotide sequence 5′-A (GGGTTA)$_3$GGG-3′ (Tel22) folded into G-quadruplex at the concentration of 4 μM (strand molarity) in analogous experimental conditions than those used in DNA FRET melting assays. The buffer system contained a 110 mM total salt concentration – 10 mM lithium cacodylate, 90 mM LiCl, 10 mM KCl at pH 7.3. Solutions of the DNA and ligands **3a-3e** at DNA/ligand ratios varying from 1:1 to 1:5 were prepared 3 h prior measurement. The CD spectra were recorded at 25 °C using a 0.5 cm-path cell, 1 nm band width, and 0.5 nm intervals. The CD spectra were averaged over two scans.

4.6. Equilibrium dialysis

Experiments were performed as previously reported [33]. The unlabeled G-quadruplex DNA (Tel22 sequence, 5′-A(GGGTTA)$_3$GGG- 3′) was purchased from IDT®, HPLC-purified and desalted. Duplex DNA from calf thymus (CT DNA), (deoxyribonucleic acid, activated, type XV), was directly purchased from Sigma Aldrich and used as provided. A 10 mM potassium phosphate buffer (pH = 7.2) with a KCl salt concentration of 100 mM was employed in the preparation of the telomeric quadruplex solution. For CT DNA, sodium phosphate buffer (10 mM, pH = 7.2) was used, in the same conditions as required in viscosity assays. Concentration of the initial water solution was determined by UV–visible at 90 °C spectrophotometry using the λ_{max} value and extinction coefficient provided by the manufacturer. For each dialysis assay, a 0.2 mL volume of each DNA in buffer (75 μM in monomeric units, tetrads or base pairs) was pipetted into individual dialysis units (Biotech Regenerated Cellulose (RC) membrane, part number 133192, Spectrum Laboratories, Inc.). The dialysis units were then placed in a beaker containing 200 mL of a 2 μM solution of compound in buffer. The beaker was covered with Parafilm and wrapped in aluminum foil, and its contents were allowed to equilibrate with continuous stirring for 24 h at room temperature (22 °C). At the end of the equilibration period, the DNA solutions inside the dialysis units were carefully transferred into microcentrifuge tubes and a 10.0% (w/v) stock solution of detergent (Triton X-100 or SDS) was added to give a final concentration of 1.0% (w/v). These solutions were allowed to equilibrate for another 2 h, after which the total concentration of the ligand (Ct) was determined by UV–visible absorbance measurements using the determined extinction coefficient for free carb-APIPs in the presence of 1.0% detergent. The concentration of free compound (C_f) was also determined spectrophotometrically using an aliquot of their dialysate solution. The amount of DNA-bound compound (C_b) was then calculated by the difference $C_b = C_t - C_f$ and apparent association constants (K_{app}) determined.

4.7. Viscosity titrations

The viscosity measurements were performed in a Visco System AVS 470 at 25 °C, using a microUbbelohde (K = 0.01) capillary viscometer [33]. Solutions of DNA (Calf thymus, CT), carb-APIPs **3a-3e**, compound **2** and appropriate controls (ethidium bromide, as classical DNA intercalator, diethylenetriamine, as a non-specific electrostatic binder) were prepared in sodium phosphate buffer (10 mM, pH = 7.2). As a control for the effect of dilution on DNA viscosity (maximum dilution ~ 2.5% volume), a blank control (titration in the absence of compound, max. 0.04% DMSO) was also run. DNA solutions (0.3–0.4 mM, in nucleotides) were equilibrated for 20 min at 25 °C and then 20 flow times were registered. Small aliquots (ca. 30–60 μL) of solutions of the tested ligand (2 mM) were added next. Before each flow time registration, the solutions were equilibrated for at least 20 min at 25 °C and then 20 flow times were measured. With the averaged flow times and the viscometer constant, the viscosities (μ) for each point were calculated, with μ_0 representing the DNA solution viscosity in the absence of compound. The viscosity results were then plotted as $(\mu/\mu_0)^{1/3}$ versus the molar ratio of bound ligand to DNA nt (r).

4.8. Cell culture and MTT colorimetric assays

Antitumor activity in cultured cells was tested as previously reported [33]. Human PC3 (prostate), HeLa (cervix) and MCF7 (breast) tumor cells were purchased from American Type Culture Collection (ATCC). Cells and culture media were: PC-3 (CRL-1435™, RPMI), HeLa (CCL-2™, DMEM), MCF7 (HTB-22™, DMEM), HFF-1 (SCRC-1041™, DMEM). Culture media was acquired from Sigma: RPMI 1640, DMEM + 10% FBS (Fetal Bovine Serum) + 10% antibiotic (penicillin/streptomycin/amphotericin B). MCF7 cells were, in addition, supplemented with insulin (Sigma, Ref. I1882, 0.001 mg/mL in 500 mL media). Cells were

maintained at 37 °C in the presence of 5% CO_2, renewing culture media three times per week. On the seeding day, when cells reached 80–100% confluence, cells were trypsinized, centrifuged and the concentration adjusted to the required experiment concentration. Cells were then seeded at a density of 10,000 cells/well into 24-well plates and treated with different concentrations of the carb-APIPs **3a-3e** or the cytotoxic agents cisplatin and 360A (typically to cover the 10 nM–100 μM range), from freshly prepared stock solutions in culture media. The experiments were run in triplicate, in a total 0.55 mL well volume. After 72 h incubation (37 °C/5% CO_2), 50 μL of MTT (5 mg/mL) was added followed by incubation for another 4 h. Then, the medium in each well was replaced by DMSO (0.5 mL) and the absorbance in every well assessed at 570 nm in an ELISA plate reader (ELX 800 Biotech Instruments, Spain). Absorbance values were normalized against negative controls (untreated cells or untreated cells with 0.15% DMSO, both in triplicate) and the percentage of viable cells versus compound logarithmic concentration was plotted. IC_{50} values were determined through the equation 1/(1 + 10ˆ(m2*(log(m1)−x))); m1 = 0.000003; m2 = 1 using Kaleidagragh™ (3.52) software.

4.9. Flow cytometry and cell cycle analysis

Flow cytometry experiments were carried out on a MACSQuant® Analyzer 10 Flow Cytometer (Miltenyi Biotech, 9 Bergisch Gladbach, Germany). Exponentially growing HeLa cells were seeded in 6-well plates in DMEM at a density of 2.5×10^5/well, and subjected to compound treatment (carb-APIP, **2**, 360A or cisplatin) at IC_{50} equivalent concentrations and control medium for 72 h. The cells were then washed with PBS and detached with 0.25% trypsin/0.2% EDTA, centrifuged at 1500 rpm for 5 min at room temperature and the pellets were mixed with 500 μL of ice-cold 70% ethanol and then kept at 4 °C for 30 min. After removing the ethanol by centrifugation, the pellets were washed with 2 mL PBS + 2% BSA and centrifuged again. The supernatants were discarded and 0.5 mL of propidium iodide solution (PI/RNASE, Immunostep) was added to cell pellets, mixed well and incubated for 15 min at room temperature before flow cytometry analysis. For each sample, 10,000 events were acquired. Results obtained were analyzed with the MacsQuantify 2.13.1 program.

Declaration of Competing Interest

The authors declare that they have no known competing financial interests or personal relationships that could have appeared to influence the work reported in this paper.

Acknowledgments

This research has received funding from Spanish MICINN and MINECO (grants PID2019-108251RB-I00/AEI/10.13039/50110001 1033, CTQ2015-72625-EXP/AEI), Consejería de Educación, Juventud y Deporte de la Comunidad de Madrid and Fondo Social Europeo (YEI, contract PEJ-2017-AI/SAL-6160, P.G.) and Universidad de Alcalá (projects CCG2016/EXP-044, CCG2018/EXP-024, CCG2020/CC-024, and UAH-AE-2017-2). We thank Daniel Diez for his contribution to the synthesis of the reported derivatives. Technical assistance by Isabel Trabado from Unidad de Cultivos UAH (CAI Medicina-Biología) is gratefully acknowledged. Graphical abstract figure was partially created by using Mol* Viewer [36] and 2HY9 PDB structure [37].

Appendix A. Supplementary material

Supplementary data to this article can be found online at https://doi.org/10.1016/j.bioorg.2022.105851.

References

[1] [a] P.N. Chopra, J.K. Sahu, Biological Significance of Imidazole-based Analogues in New Drug Development, Curr. Drug Discov. Technol. 17 (2020) 574–584, https://doi.org/10.2174/1570163816666190320123340;
[b] R. Rossi, M. Ciofalo, An Updated Review on the Synthesis and Antibacterial Activity of Molecular Hybrids and Conjugates Bearing Imidazole Moiety, Molecules 25 (2020) 5133, https://doi.org/10.3390/molecules25215133;
[c] D.G. Daraji, N.P. Prajapati, H.D. Patel, Synthesis and Applications of 2-Substituted Imidazole and Its Derivatives: A Review, J. Heterocyclic Chem. 56 (2019) 2299–2317, https://doi.org/10.1002/jhet.3641;
[d] L. Zhang, X.-M. Peng, G.L.V. Damu, R.-X. Geng, C.-H. Zhou, Comprehensive Review in Current Developments of Imidazole-Based Medicinal Chemistry, Med. Res. Rev. 34 (2014) 340–437, https://doi.org/10.1002/med.21290;
[e] A. Verma, S. Joshi, D. Singh, Imidazole: Having Versatile Biological Activities, Journal of Chemistry, Volume 2013, Article ID 329412 (2013), https://doi.org/10.1155/2013/329412.

[2] [a] K. Kappler, T. Hennet, Emergence and significance of carbohydrate-specific antibodies, Genes Immun. 21 (2020) 224–239, https://doi.org/10.1038/s41435-020-0105-9;
[b] X. Sun, G. Stefanetti, F. Bertid, D.L. Kaspera, Polysaccharide structure dictates mechanism of adaptive immune response to glycoconjugate vaccines, PNAS 116 (2019) 193–198, https://doi.org/10.1073/pnas.1816401115;
[c] A. Varki, Biological roles of glycans, Glycobiology 27 (2017) 3–47, https://doi.org/10.1093/glycob/cww086;
[d] H. Ghazarian, B. Idoni, B. Oppenheimer, A glycobiology review: carbohydrates, lectins and implications in cancer therapeutics, Acta Histochem. 113 (2011) 236–247.

[3] [a] M. Rose, J.T. Burgess, K. O'Byrne, D.J. Richard, E. Bolderson, PARP Inhibitors: Clinical Relevance, Mechanisms of Action and Tumor Resistance, Front. Cell Dev. Biol. 8 (2020) 564601, https://doi.org/10.3389/fcell.2020.564601;
[b] S. Boussios, P. Karihtala, M. Moschetta, C. Abson, A. Karathanasi, N. Zakynthinakis-Kyriakou, J.E. Ryan, M. Sheriff, E. Rassy, N. Pavlidis, Veliparib in ovarian cancer: a new synthetically lethal therapeutic approach, Invest. New Drugs. 38 (2020) 181–193, https://doi.org/10.1007/s10637-019-00867-4.

[4] [a] S.S. Thakare, G. Chakraborty, S. Kothavale, S. Mula, A.K. Ray, N. Sekar, Proton Induced Modulation of ICT and PET Processes in an Imidazo-phenanthroline Based BODIPY Fluorophores, J. Fluoresc. 27 (2017) 2313–2322, https://doi.org/10.1007/s10895-017-2173-4;
[b] Y.-L. Pan, Z.-B. Cai, L. Bai, F.-F. Ma, S.-L. Li, Y.-P. Tian, Green synthesis and photophysical properties of novel 1H-imidazo[4,5-f][1,10]phenanthroline derivatives with blue/cyan two-photon excited fluorescence, Tetrahedron 73 (2017) 2886–2893, https://doi.org/10.1016/j.tet.2017.03.075;
[c] C. Guo, M. Xu, C. Chen, Z. Zheng, J. Chen, R. Geng, Q. Wang, A novel 1,10-phenanthroline-based fluorescent probe for selective detection of D- 3-HB, ChemXpress 9 (2016) 114;
[d] P. Scharf, B. Jash, J.A. Kuriappan, M.P. Waller, J. Müller, Sequence-Dependent Duplex Stabilization upon Formation of a Metal-Mediated Base Pair, Chem. Eur. J. 22 (2016) 295–301, https://doi.org/10.1002/chem.201503405;
[e] A. Yoldas, F. Algi, An imidazo-phenanthroline scaffold enables both chromogenic Fe(II) and fluorogenic Zn(II) detection, RSC Adv. 5 (2015) 7868–7873, https://doi.org/10.1039/C4RA14182B;
[f] D.-D. Sun, W.-Z. Wang, J.-W. Mao, W.-J. Mei, J. Liu, Imidazo[4,5-f][1,10] phenanthroline derivatives as inhibitor of c-myc gene expression in A549 cells via NF-?B pathway, Bioorg. Med. Chem. Lett. 22 (2012) 102–105, https://doi.org/10.1016/j.bmcl.2011.11.063;
[g] N.N. Sergeeva, M. Donnier-Marechal, G.M. Vaz, A.M. Davies, M.O. Senge, Simple but powerful: Phenanthroline-based small molecules for cellular imaging and cancer screening, Bioorg. Med. Chem. Lett. 21 (2011) 4385–4388, https://doi.org/10.1016/j.bmcl.2011.06.051;
[h] J.-F. Lee, Y.-C. Chen, J.-T. Lin, C.-C. Wu, C.-Y. Chen, C.-A. Dai, C.-Y. Chao, H.-L. Chen, W.-B. Liau, Blue light-emitting and electron-transporting materials based on dialkyl-functionlized anthracene imidazophenanthrolines, Tetrahedron 67 (2011) 1696–1702, https://doi.org/10.1016/j.tet.2010.12.059.

[5] [a] E.J. Anthony, E.M. Bolitho, H.E. Bridgewater, O.W.L. Carter, J.M. Donnelly, C. Imberti, E.C. Lant, F. Lermyte, R.J. Needham, M. Palau, P.J. Sadler, H. Shi, F.-X. Wang, W.-Y. Zhang, Z. Zhang, Metallodrugs are unique: opportunities and challenges of discovery and development, Chem. Sci. 11 (2020) 12888–12917, https://doi.org/10.1039/D0SC04082G;
[b] A. Bergamo, P.J. Dyson, G. Sava, The mechanism of tumour cell death by metal-based anticancer drugs is not only a matter of DNA interactions, Coordin, Chem. Rev. 360 (2018) 17–33, https://doi.org/10.1016/j.ccr.2018.01.009;
[c] V. Brabec, J. Kasparkova, Ruthenium coordination compounds of biological and biomedical significance. DNA binding agents, Coordin. Chem. Rev. 376 (2018) 75–94, https://doi.org/10.1016/j.ccr.2018.07.012.

[6] [a] B. Kar, U. Das, S.D. De, S. Pete, A.S. Sharma, R. Nilmadhab, S.K. Ashok Kumar, D. Panda, P. Paira, GSH-resistant and highly cytoselective ruthenium(ii)-p-cymene-(imidazo[4,5-f][1,10]phenanthrolin-2-yl)phenol complexes as potential anticancer agents, Dalton Trans. 50 (2021) 10369–10373, https://doi.org/10.1039/D1DT01604K;
[b] S. De, R.S. Kumar, A. Gauthaman, S.K. Ashok Kumar, P. Paira, A. Moorthy, S. Banerjee, Luminescent ruthenium(II)-para-cymene complexes of aryl substituted imidazo-1,10-phenanthroline as anticancer agents and the effect of remote substituents on cytotoxic activities, Inorgan. Chim. Acta 515 (2021) 120066, https://doi.org/10.1016/j.ica.2020.120066;
[c] U. Das, B. Kar, S. Pete, P. Paira, Ru(II), Ir(III), Re[i] and Rh(III) based

complexes as next generation anticancer metallopharmaceuticals, Dalton Trans. 50 (2021) 11259–11290, https://doi.org/10.1039/D1DT01326B;
[d] A. Mondal, P. Paira, Hypoxia efficient and glutathione-resistant cytoselective ruthenium(ii)-p-cymene-arylimidazophenanthroline complexes: biomolecular interaction and live cell imaging, Dalton Trans. 49 (2020) 12865–12878, https://doi.org/10.1039/D0DT02069A;
[e] B. Sarkar, A. Mondal, Y. Madaan, N. Roy, A. Moorthy, Y.-C. Kuo, P. Paira, Luminescent anticancer ruthenium(II)-p-cymene complexes of extended imidazophenanthroline ligands: synthesis, structure, reactivity, biomolecular interactions and live cell imaging, Dalton Trans. 48 (2019) 12257–12271, https://doi.org/10.1039/C9DT00921C;
[f] X.-L. Zhao, H.-Q. Zhao, X.-X. Xu, Z.-S. Li, K.-Z. Wang, Inducement and stabilization of G-quadruplex DNA by a thiophene-containing dinuclear ruthenium (II) complex, J. Coord. Chem. 70 (2017) 2094–2112, https://doi.org/10.1080/00958972.2017.1322694;
[g] Y. Chen, Q. Wu, X. Wang, Q. Xie, Y. Tang, Y. Lan, S. Zhang, W. Mei, Microwave-Assisted Synthesis of Arene Ru(II) Complexes Induce Tumor Cell Apoptosis Through Selectively Binding and Stabilizing *bcl*-2 G-Quadruplex DNA, Materials 9 (2016) 386, https://doi.org/10.3390/ma9050386;
[h] B. Senthamarai Kannan, D. Suresh Kumar, R. Host Antony David, A. Stalin, S. Ignacimuthu, Acid–base effects, light emission, DNA-binding and photocleavage studies of oligo-homonuclear ruthenium(II) complexes and their computational study, Inorg. Chim. Acta 432 (2015) 158–168, https://doi.org/10.1016/j.ica.2015.03.042;
[i] J. Zhang, Q. Yu, Q. Li, L. Yang, L. Chen, Y. Zhou, J. Liu, A ruthenium(II) complex capable of inducing and stabilizing bcl-2 G-quadruplex formation as a potential cancer inhibitor, J. Inorg. Biochem. 134 (2014) 1–11, https://doi.org/10.1016/j.jinorgbio.2013.12.005;
[j] C. Fan, O. Wu, T. Chen, Y. Zhang, W. Zheng, Q. Wang, W. Mei, Arene ruthenium(II) complexes induce S-phase arrest in MG-63 cells through stabilization of *c-Myc* G-quadruplex DNA, Med. Chem. Commun. 5 (2014) 597–602, https://doi.org/10.1039/C3MD00367A;
[k] Q. Wu, T. Chen, Z. Zhang, S. Liao, X. Wu, J. Wu, W. Mei, Y. Chen, W. Wu, L. Zenha, W. Zheng, Microwave-assisted synthesis of arene ruthenium(II) complexes [(?6 -RC6H5)Ru(m-MOPIP)Cl]Cl (R = -H and -CH3) as groove binder to *c-myc* G4 DNA, Dalton Trans. 43 (2014) 9216–9225, https://doi.org/10.1039/C3DT53635A;
[l] Y.-C. Wang, C. Qian, Z.-L. Peng, X.-J. Hou, L.-L. Wang, H. Chao, L.-N. Ji, Dual Topoisomerase I and II poisoning by chiral Ru(II) complexes containing 2-thiophenyl imidazo[4,5-f][1,10]phenanthroline derivatives, J. Inorg. Biochem. 130 (2014) 15–27, https://doi.org/10.1016/j.jinorgbio.2013.09.015;
[m] Q. Li, J. Zhang, L. Yang, Q. Yu, Q. Chen, X. Qin, F. Le, Q. Zhang, J. Liu, Stabilization of G-quadruplex DNA and inhibition of telomerase activity studies of ruthenium(II) complexes, J. Inorg. Biochem. 130 (2014) 122–129, https://doi.org/10.1016/j.jinorgbio.2013.10.006;
[n] M. Stephenson, C. Reichardt, M. Pinto, M. Wächtler, T. Sainuddin, G. Shi, H. Yin, S. Monro, E. Sampson, B. Dietzek, S.A. McFarland, Ru(II) Dyads Derived from 2-(1-Pyrenyl)-1H-imidazo[4,5-f][1,10]phenanthroline: Versatile Photosensitizers for Photodynamic Applications, J. Phys. Chem. A 118 (2014) 10507–10521, https://doi.org/10.1021/jp504330s;
[o] H.-L. Huang, Y.-J. Liu, C.-H. Zeng, L.-X. He, F.-H. Wu, In vitro cytotoxicity, apoptosis, DNA-binding, and antioxidant activity studies of ruthenium (II) complexes, DNA Cell Biol. 29 (2010) 261–270, https://doi.org/10.1089/dna.2009.0979.

[7] [a] C. Alexander, N.U. Prajith, P.V. Priyanka, A. Nithyakumar, N.A. Samy, Dinuclear platinum(II) complexes of imidazophenanthroline-based bridging ligands as potential anticancer agents: synthesis, characterization, and in vitro cytotoxicity studies, J. Biol. Inorg. Chem. 24 (2019) 405–418, https://doi.org/10.1007/s00775-019-01656-3;
[b] C. Alexander, A. Nithyakumar, M.W.B. Paul, N.A. Samy, Platinum(II) complexes of imidazophenanthroline-based polypyridine ligands as potential anticancer agents: synthesis, characterization, in vitro cytotoxicity studies and a comparative ab initio, and DFT studies with cisplatin, carboplatin, and oxaliplatin, J. Biol. Inorg. Chem. 23 (2018) 833–848, https://doi.org/10.1007/s00775-018-1579-z;
[c] X.J. Luo, Q.P. Qin, Y.L. Li, Y.C. Liu, Z.F. Chen, H. Liang, Three platinum(II) complexes of 2-(methoxy-phenyl)-imidazo-[4,5-f]-[1,10]phenanthroline: Cell apoptosis induction by sub-G1 phase cell cycle arrest and G-quadruplex binding properties, Inorg. Chem. Commun. 46 (2014) 176–179, https://doi.org/10.1016/j.inoche.2014.05.032;
[d] H.-J. Zhong, W. Wang, T.-S. Kang, H. Yan, Y. Yang, L. Xu, Y. Wang, D.-L. Ma, C.-H. Leung, A Rhodium(III) Complex as an Inhibitor of Neural Precursor Cell Expressed, Developmentally Down-Regulated 8-Activating Enzyme with in Vivo Activity against Inflammatory Bowel Disease, J. Med. Chem. 60 (2017) 497–503, https://doi.org/10.1021/acs.jmedchem.6b00250;
[e] P. Ying, P. Zeng, J. Lu, N. Yang, H. Chen, Photocleavage Properties and DNA-Binding Studies of Oxovanadium Complexes Incorporating 2-(2-Hydroxybenzylidene amino) Isoindoline-1,3-Dione and Fluoro-Phenanthroline Derivatives, Open, J. Inorg. Chem. 4 (2014) 51–63, https://doi.org/10.4236/ojic.2014.44007.

[8] [a] M.-A. Schmid, M. Rentschler, W. Frey, S. Tschierlei, M. Karnahl, Imidazo-Phenanthroline Ligands as a Convenient Modular Platform for the Preparation of Heteroleptic Cu[i] Photosensitizers, Inorganics 6 (2018) 134, https://doi.org/10.3390/inorganics6040134;
[b] T. Cardinaels, J. Ramaekers, P. Nockemann, K. Driesen, K. Van Hecke, L. Van Meervelt, S. Lei, S. De Feyter, D. Guillon, B. Donnio, K. Binnemans, Imidazo[4,5-f]-1,10-phenanthrolines: Versatile Ligands for the Design of Metallomesogens, Chem. Mater. 20 (2008) 1278–1291, https://doi.org/10.1021/cm070637i;
[c] H.-P. Fang, Y.-H. Wu, H.-C. Lin, Synthesis and study of novel supramolecular nanocomposites containing aryl-imidazo-phenanthroline-based metallo-polymers (H-donors) and surface-modified ZnO nanoparticles (H-acceptors), Tetrahedron 69 (2013) 293–301, https://doi.org/10.1016/j.tet.2012.10.031.

[9] [a] N. Kosiol, S. Juranek, P. Brossart, A. Heine, K. Paeschke, G-quadruplexes: a promising target for cancer therapy, Mol. Cancer 20 (2021) 40, https://doi.org/10.1186/s12943-021-01328-4;
[b] J. Tan, L. Lan, The DNA secondary structures at telomeres and genome instability, Cell Biosci. 10 (2020) 47, https://doi.org/10.1186/s13578-020-00409-z;
[c] A.K. Mukherjee, S. Sharma, S. Chowdhury, Non-duplex G-Quadruplex Structures Emerge as Mediators of Epigenetic Modifications, Trends Genet. 35 (2019) 129–135, https://doi.org/10.1016/j.tig.2018.11.001;
[d] M.P. O'Hagan, J.C. Morales, M.C. Galan, Binding and Beyond: What Else Can G-Quadruplex Ligands Do? Eur. J. Org. Chem. (2019) 4995–5017, https://doi.org/10.1002/ejoc.201900692;
[e] T. Tian, Y.Q. Chen, S.R. Wang, X. Zhou, G-Quadruplex: A Regulator of Gene Expression and Its Chemical Targeting, Chem. 4 (2018) 1314–1344, https://doi.org/10.1016/j.chempr.2018.02.014;
[f] R. Hänsel-Hertsch, M. Di Antonio, S. Balasubramanian, DNA G-quadruplexes in the human genome: Detection, functions and therapeutic potential, Nat. Rev. Mol. Cell Biol. 18 (2017) 279–284, https://doi.org/10.1038/nrm.2017.3;
[g] D. Monchaud, Quadruplex-DNA: structures, functions and detection, Med. Sci. (Paris) 33 (2017) 1042–1045, https://doi.org/10.1051/medsci/20173312008.

[10] [a] A. Sengupta, A. Ganguly, S. Chowdhury, Promise of G-quadruplex structure binding ligands as epigenetic modifiers with anti-cancer effects, Molecules 24 (2019) 582, https://doi.org/10.3390/molecules24030582;
[b] R. Rigo, M. Palumbo, C. Sissi, G-quadruplexes in human promoters: A challenge for therapeutic applications, Biochim. Biophys. Acta 2017 (5 Pt B) (1861) 1399–1413, https://doi.org/10.1016/j.bbagen.2016.12.024;
[c] S. Neidle, Quadruplex nucleic acids as targets for anticancer therapeutics, Nat. Rev. Chem. 1 (2017) 41, https://doi.org/10.1038/s41570-017-0041.[d] D. Monchaud, (Ed.) Biological Relevance & Therapeutic Applications of DNA- & RNA-Quadruplexes, Future Science, London, 2015. https://doi.org/10.4155/9781910419687.

[11] [a] S. Lang, X. Huang, Carbohydrate conjugates in vaccine developments, Front. Chem. 8 (2020) 284, https://doi.org/10.3389/fchem.2020.00284;
[b] R. Mettu, C.-Y. Chen, C.-Y. Wu, Synthetic carbohydrate-based vaccines: challenges and opportunities, J. Biomed. Sci. 27 (2020) 9, https://doi.org/10.1186/s12929-019-0591-0;
[c] K.-T. Jin, H.-R. Lan, X.-Y. Chen, S.-B. Wang, X.-J. Ying, Y. Lin, X.-Z. Mou, Recent advances in carbohydrate-based cancer vaccines, Biotechnol. Lett. 41 (2019) 641–650, https://doi.org/10.1007/s10529-019-02675-5;
[d] D. Feng, A.S. Shaikh, F. Wang, Recent advance in tumor-associated carbohydrate antigens (TACAs)-based antitumor vaccines, ACS Chem. Biol. 11 (2016) 850–863, https://doi.org/10.1021/acschembio.6b00084;
[e] S.J. Danishefsky, J.A. Allen, From the laboratory to the clinic: a retrospective on fully synthetic carbohydrate-based anticancer vaccines, Angew. Chem. Int. Ed. 39 (2000) 836–863, https://doi.org/10.1002/(sici)1521-3773(20000303)39:5<836::aid-anie836>3.0.co;2-i.

[12] [a] P. Valverde, A. Ardá, N.C. Reichardt, J. Jiménez-Barbero, A. Gimeno, Glycans in drug discovery, Medchemcomm. 10 (2019) 1678–1691, https://doi.org/10.1039/c9md00292h;
[b] J. Shelton, X. Lu, J.A. Hollenbaugh, J.H. Cho, F. Amblard, R.F. Schinazi, Metabolism, biochemical actions, and chemical synthesis of anticancer nucleosides, nucleotides, and base analogs, Chem. Rev. 116 (2016) 14379–14445, https://doi.org/10.1021/acs.chemrev.6b00209;
[c] G.F. Weber, Molecular Therapies of Cancer, Springer, Heidelberg, 2015;
[d] D.B. Werz, P.H. Seeberger, Carbohydrates as the next frontier in pharmaceutical research, Chem. Eur. J. 11 (2005) 3194–3206, https://doi.org/10.1002/chem.200500025;
[e] Y.M. Chabre, R. Roy, Design and creativity in synthesis of multivalent neoglycoconjugates, Adv Carbohydr Chem Biochem. 63 (2010) 165–393, https://doi.org/10.1016/s0065-2318(10)63006-5.

[13] [a] A. Harland, X. Liu, M. Ghirardello, M.C. Galan, C.M. Perks, K.M. Kurian, Glioma Stem-Like Cells and Metabolism: Potential for Novel Therapeutic Strategies, Front. Oncol. 11 (2021) 743814, https://doi.org/10.3389/fonc.2021.743814;
[b] C. Granchi, S. Fortunato, F. Minutolo, Anticancer agents interacting with membrane glucose transporters, MedChemComm. 7 (2016) 1716–1729, https://doi.org/10.1039/C6MD00287K;
[c] H. Zhang, J. Xiang, H. Hu, Y. Liu, F. Yang, G. Shen, Y. Tang, C. Chen, Selective recognition of specific G-quadruplex vs. duplex DNA by a phenanthroline derivative, Int. J. Biol. Macromol. 78 (2015) 149–156, https://doi.org/10.1016/j.ijbiomac.2015.03.034;
[d] D. Zhang, J. Li, F. Wang, J. Hu, S. Wang, Y. Sun, 2-Deoxy-D-glucose targeting of glucose metabolism in cancer cells as a potential therapy, Cancer Lett. 355 (2014) 176–183, https://doi.org/10.1016/j.canlet.2014.09.003;
[e] E.C. Calvaresi, P.J. Hergenrother, Glucose conjugation for the specific targeting and treatment of cancer, Chem. Sci. 4 (2013) 2319–2333, https://doi.org/10.1039/C3SC22205E.

[14] [a] M. Arévalo-Ruiz, S. Amrane, F. Rosu, E. Belmonte-Reche, P. Peñalver, J.-L. Mergny, J.C. Morales, Symmetric and dissymmetric carbohydrate-phenyl ditriazole derivatives as DNA G-quadruplex ligands: Synthesis, biophysical studies

and antiproliferative activity, Bioorg. Chem. 99 (2020) 103786, https://doi.org/10.1016/j.bioorg.2020.103786;
[b] M. Arévalo-Ruiz, F. Doria, E. Belmonte-Reche, A. De Rache, J. Campos-Salinas, R. Lucas, E. Falomir, M. Carda, J.M. Pérez-Victoria, J.-L. Mergny, M. Freccero, J. C. Morales, Synthesis, Binding Properties, and Differences in Cell Uptake of G-Quadruplex Ligands Based on Carbohydrate Naphthalene Diimide Conjugates, Chem. Eur. J. 23 (2017) 2157–2164, https://doi.org/10.1002/chem.201604886;
[c] S.T.G. Street, D.N. Chin, G.J. Hollingworth, M. Berry, J.C. Morales, M. C. Galan, Divalent Naphthalene Diimide Ligands Display High Selectivity for the Human Telomeric G-quadruplex in K+ Buffer, Chem. Eur. J. 23 (2017) 6953–6958, https://doi.org/10.1002/chem.201700140;
[d] I. Gómez-Pinto, E. Vengut-Climent, R. Lucas, A. Aviñó, R. Reitja, C. González, J.C. Morales, Carbohydrate–DNA Interactions at G-Quadruplexes: Folding and Stability Changes by Attaching Sugars at the 5'-End, Chem. Eur. J. 19 (2013) 1920–1927, https://doi.org/10.1002/chem.201203902;
[e] M. Di Antonio, G. Biffi, A. Mariani, E.-A. Raiber, R. Rodriguez, S. Balasubramanian, Selective RNA Versus DNA G-Quadruplex Targeting by In Situ Click Chemistry, Angew. Chem. Int. Ed. Engl. 51 (2012) 11073–11078, https://doi.org/10.1002/ange.201206281;
[f] N. Ranjan, K.F. Andreasen, S. Kumar, D. Hyde-Volpe, D.P. Arya, Aminoglycoside Binding to Oxytricha nova Telomeric DNA, Biochemistry 49 (2010) 9891–9903, https://doi.org/10.1021/bi101517e;
[g] A. Bugaut, K. Jantos, J.-L. Wietor, R. Rodriguez, J.K.M. Sanders, S. Balasubramanian, Exploring the Differential Recognition of DNA G-Quadruplex Targets by Small Molecules Using Dynamic Combinatorial Chemistry, Angew. Chem. Int. Ed. 47 (2008) 2677–2680, https://doi.org/10.1002/ange.200705589.

[15] [a] K. Duskova, L. Gude, M.S. Arias-Pérez, N-Phenanthroline glycosylamines: synthesis and copper(II) complexes, Tetrahedron 70 (2014) 1071–1076, https://doi.org/10.1016/j.tet.2013.12.044;
[b] K. Duskova, S. Sierra, M.S. Arias-Pérez, L. Gude, Human telomeric G-quadruplex DNA interactions of N-phenanthroline glycosylamine copper(II) complexes, Bioorg. Med. Chem. 24 (2016) 33–41, https://doi.org/10.1016/j.bmc.2015.11.037;
[c] S. Jäger, L. Gude, M.S. Arias-Pérez, 4,5-Diazafluorene N-glycopyranosyl hydrazones as scaffolds for potential bioactive metallo-organic compounds: Synthesis, structural study and cytotoxic activity, Bioorg. Chem. 81 (2018) 405–413, https://doi.org/10.1016/j.bioorg.2018.08.019.

[16] [a] V. Ramu, S. Gautam, A. Garai, P. Kondaiah, A.R. Chakravarty, Glucose-Appended Platinum(II)-BODIPY Conjugates for Targeted Photodynamic Therapy in Red Light, Inorg. Chem. 57 (2018) 1717–1726, https://doi.org/10.1021/acs.inorchem.7b02249;
[b] J. Ma, X. Yang, W. Hao, Z. Huang, X. Wang, P.G. Wang, Mono-functionalized glycosylated platinum(IV) complexes possessed both pH and redox dual-responsive properties: Exhibited enhanced safety and preferentially accumulated in cancer cells in vitro and in vivo, Eur. J. Med. Chem. 128 (2017) 45–55, https://doi.org/10.1016/j.ejmech.2017.01.032;
[c] Y. Mikata, M. Gottschaldt, Metal Complexes of Carbohydrate-targeted Ligands, in: T. Storr (Ed.), Medicinal Inorganic Chemistry in Ligand Design in Medicinal Inorganic Chemistry, Wiley & Sons, Chichester, 2014, pp. 145–174;
[d] S. Spreckelmeyer, C. Orvig, A. Casini, Cellular Transport Mechanisms of Cytotoxic Metallodrugs: An Overview beyond Cisplatin, Molecules 19 (2014) 15584–15610, https://doi.org/10.3390/molecules191015584;
[e] B. Banik, K. Somyajit, A. Hussain, G. Nagaraju, A.R. Chakravarty, Carbohydrate-appended photocytotoxic (imidazophenanthroline)-oxovanadium (IV) complexes for cellular targeting and imaging, Dalton Trans. 43 (2014) 1321–1331, https://doi.org/10.1039/C3DT52087K.

[17] [a] P. Norris, Pyranose N-glycosyl amines: emerging targets with diverse biological potential, Curr. Top. Med. Chem. 8 (2008) 101–113, https://doi.org/10.2174/156802608783378837;
[b] A.R. Genady, M.E. El-Zaria, Novel glycosylated carboranylquinazolines for boron neutron capture therapy of tumors: synthesis, characterization, and in vitro toxicity studies, Appl. Organometal. Chem. (2008) 227–232, https://doi.org/10.1002/aoc.1376;
[c] M.K. Dhinakaran, T.M. Das, Studies on a novel class of triaryl pyridine N-glycosylamine amphiphiles as super gelators, Org. Biomol. Chem. 10 (2012) 2077–2083, https://doi.org/10.1039/C2OB06834F.

[18] [a] M. Prudhomme, Biological targets of antitumor indolocarbazoles bearing a sugar moiety, Curr. Med. Chem.: Anti-Cancer Agents 4 (2004) 509–521, https://doi.org/10.2174/1568011043352650;
[b] F. Animati, M. Berettoni, M. Bigioni, M. Binaschi, A. Cipollone, C. Irrissuto, F. Nardelli, L. Olivieri, Synthesis and biological evaluation of rebeccamycin analogues modified at the imide moiety, Bioorg. Med. Chem. Lett. 22 (2012) 5013–5017, https://doi.org/10.1016/j.bmcl.2012.06.016.

[19] [a] M.B. Fusaro, V. Chagnault, D. Postel, Synthesis of glycosylamines and glyconamides using molecular iodine, Tetrahedron 69 (2013) 542–550, https://doi.org/10.1016/j.tet.2012.11.027;
[b] M. Rajasekar, S.M. Khan, S.N. Devaraj, T.M. Das, Design, synthesis, and biological evaluation of a novel class of fluorescein-based N-glycosylamines, Carbohydr. Res. 346 (2011) 1776–1785, https://doi.org/10.1016/j.carres.2011.06.001;
[c] M.Y. Gokhale, L.E. Kirsch, Glycosylation of aromatic amines III: Mechanistic implications of the pH-dependent glycosylation of various aromatic amines (kynurenine, 2'-aminoacetophenone, daptomycin, and sulfamethoxzaole), J. Pharm. Sci. 98 (2009) 4639–4649, https://doi.org/10.1002/jps.21769;
[d] R.I. Kublashvili, M.O. Labartkava, K.P. Giorgadze, D.Sh. Ugrekhelidze, Synthesis and characterization of N-tolyglycosylamines, Chem. Nat. Compd. 44 (2008) 413–415, https://doi.org/10.1007/s10600-008-9095-y;
[e] N. Bridiau, M. Benmansour, M.D. Legoy, T. Maugard, One-pot stereoselective synthesis of ß-N-aryl-glycosides by N-glycosylation of aromatic amines: application to the synthesis of tumor-associated carbohydrate antigen building blocks, Tetrahedron 63 (2007) 4178–4183, https://doi.org/10.1016/j.tet.2007.02.092;
[f] W. Du, Y. Hu, Synthesis of Fully Protected N-Arylglycosylamines and Factors Affecting the Configuration of C1-Substituents of N-Arylglycosylamines, Synth. Commun. 34 (2004) 2987–2992, https://doi.org/10.1081/SCC-200026656;
[g] G. Rajsekhar, C.P. Rao, P. Saarenketo, E. Kolehmainen, K. Rissanen, Glycosylamines of 4,6-O-butylidene-a-D-glucopyranose: synthesis and characterization of glycosylamines, and the crystal structure of 4,6-O-butylidene-N-(o-chlorophenyl)-ß-D-glucopyranosylamine, Carbohydr. Res. 337 (2002) 187–194, https://doi.org/10.1016/S0008-6215(01)00311-1;
[h] X. Qian, Z. Li, G. Song, Syntheses and activities as trehalase inhibitors of N-arylglycosylamines derived from fluorinated anilines, Carbohydr. Res. 336 (2001) 79–82, https://doi.org/10.1016/S0008-6215(01)00126-4;
[i] T.M. Das, C.P. Rao, E. Kolehmainen, Synthesis and characterisation of N-glycosyl amines from the reaction between 4,6-O-benzylidene-D-glucopyranose and substituted aromatic amines and also between 2-(o-aminophenyl) benzimidazole and pentoses or hexoses Carbohydr, Res. 334 (2001) 261–269, https://doi.org/10.1016/S0008-6215(01)00202-6.

[20] [a] R.J. Batchelor, D.F. Green, B.D. Johnston, B.O. Patrick, B.M. Pinto, Conformational preferences in glycosylamines. Implications for the exo-anomeric effect, Carbohydr. Res. 330 (2001) 421–426, https://doi.org/10.1016/S0008-6215(00)00304-9;
[b] J.O. Duus, C.H. Gotfredsen, K. Bock, Carbohydrate structural determination by NMR spectroscopy: modern methods and limitation, Chem. Rev. 100 (2000) 4589–4614, https://doi.org/10.1021/cr990302n.

[21] [a] F. Su, Z. Sun, W. Su, X. Liang, NMR investigation and theoretical calculations on the tautomerism of benzimidazole compounds 2018, J. Mol. Struct. 1173 (2018) 690–696, https://doi.org/10.1016/j.molstruc.2018.07.038;
[b] C.I. Nieto, P. Cabildo, M.A. García, R.M. Claramunt, I. Alkorta, J. Elguero, An experimental and theoretical NMR study of NH-benzimidazoles in solution and in the solid state: proton transfer and tautomerism, Beilstein J. Org. Chem. 10 (2014) 1620–1629, https://doi.org/10.3762/bjoc.10.168.

[22] [a] D. Hanahan, R.A. Weinberg, Hallmarks of cancer: the next generation, Cell 144 (2011) 646–674, https://doi.org/10.1016/j.cell.2011.02.013;
[b] S. Neidle, Human telomeric G-quadruplex: The current status of telomeric G-quadruplexes as therapeutic targets in human cancer, FEBS J. 277 (2010) 1118–1125, https://doi.org/10.1111/j.1742-4658.2009.07463.x.

[23] [a] A. De Cian, L. Guittat, M. Kaiser, B. Saccà, S. Amrane, A. Bourdoncle, P. Alberti, M.-P. Teulade-Fichou, L. Lacroix, J.L. Mergny, Fluorescence-based melting assays for studying quadruplex ligands, Methods 42 (2007) 183–195. https://doi:10.1016/j.ymeth.2006.10.004;
[b] D. Renciuk, J. Zhou, L. Beaurepaire, A. Guédin, A. Bourdoncle, J.L. Mergny, A FRET-based screening assay for nucleic acid ligands, Methods 57 (2012) 122–128, https://doi.org/10.1016/j.ymeth.2012.03.020;
[c] R. Kieltyka, P. Englebienne, J. Fakhoury, C. Autexier, N. Moitessier, H. F. Sleiman, A platinum supramolecular square as an effective G-quadruplex binder and telomerase inhibitor, J. Am. Chem. Soc. 130 (2008) 10040–10041, https://doi.org/10.1021/ja8014023.

[24] [a] A. Randazzo, G.P. Spada, M.W. da Silva, Circular dichroism of quadruplex structures, Top. Curr. Chem. 330 (2013) 67–86, https://doi.org/10.1007/128_2012_331;
[b] A.I. Karsisiotis, N.M. Hessari, E. Novellino, G.P. Spada, A. Randazzo, M. Webba da Silva, Topological characterization of nucleic acid G-quadruplexes by UV absorption and circular dichroism, Angew. Chem. Int. Ed. Engl. 50 (2011) 10645–10648, https://doi.org/10.1002/anie.201105193;
[c] R. del Villar-Guerra, J.O. Trent, J.B. Chaires, G-Quadruplex Secondary Structure Obtained from Circular Dichroism Spectroscopy, Angew. Chem. Int. Ed. 57 (2018) 7171–7175, https://doi.org/10.1002/anie.201709184.

[25] [a] S. Paramasivan, I. Rujan, P.H. Bolton, Circular dichroism of quadruplex DNAs: applications to structure, cation effects and ligand binding, Methods 43 (2007) 324–331, https://doi.org/10.1016/j.ymeth.2007.02.009;
[b] I. Bessi, C. Bazzicalupi, C. Richter, H.R.A. Jonker, K. Saxena, C. Sissi, M. Chioccioli, S. Bianco, A.R. Bilia, H. Schwalbe, P. Gratteri, Spectroscopic, molecular modeling, and NMR-spectroscopic investigation of the binding mode of the natural alkaloids berberine and sanguinarine to human telomeric G-quadruplex DNA, ACS Chem. Biol. 7 (2012) 1109–1119, https://doi.org/10.1021/cb300096g.

[26] [a] A. Ambrus, D. Chen, J. Dai, T. Bialis, R.A. Jones, D. Yang, Human telomeric sequence forms a hybrid-type intramolecular G-quadruplex structure with mixed parallel/antiparallel strands in potassium solution, Nucleic Acids Res. 34 (2006) 2723–2735, https://doi.org/10.1093/nar/gkl348;
[b] K.N. Luu, A.T. Phan, V. Kuryavyi, L. Lacroix, D.J. Patel, Structure of the Human Telomere in K+ Solution: An Intramolecular (3 + 1) G-Quadruplex Scaffold, J. Am. Chem. Soc. 128 (2006) 9963–9970, https://doi.org/10.1021/ja062791w.

[27] [a] J. Ren, J.B. Chaires, Rapid screening of structurally selective ligand binding to nucleic acids, Methods Enzymol. 340 (2001) 99–108, https://doi.org/10.1016/S0076-6879(01)40419-8;
[b] J.B. Chaires, Nucleic acid binding molecules: A Competition Dialysis Assay for the Study of Structure-Selective Ligand Binding to Nucleic Acids, in: S.L. Beaucage, D.E. Bergstrom, G.D. Glick, R.A. Jones (Eds.), Current Protocols in Nucleic Acid Chemistry, John Wiley & Sons, New York, 2002, pp. 831–838, https://doi.org/10.1002/0471142700.nc0803s11;
[c] J.B. Chaires, Structural Selectivity of Drug-Nucleic Acid Interactions Probed by

Competition Dialysis, in: M.J. Waring, J.B. Chaires (Eds.), DNA Binders and Related Subjects. Topics in Current Chemistry 253, Springer, Berlin, Heidelberg, 2005, pp. 33–53, https://doi.org/10.1007/b100441.
[28] K.E. van Holde, W.C. Johnson, P.S. Ho, Principles of Physical Biochemistry, Prentice Hall, New Jersey, 1998.
[29] W. Muller, D.M. Crothers, Interactions of Heteroaromatic Compounds with Nucleic Acids, Eur. J. Biochem. 54 (1975) 267–277, https://doi.org/10.1111/j.1432-1033.1975.tb04138.x.
[30] D. Suh, J.B. Chaires, Criteria for the mode of binding of DNA binding agents, Bioorg. Med. Chem. 3 (1995) 723–728, https://doi.org/10.1016/0968-0896(95)00053-J.
[31] G. Cohen, H. Eisenberg, Viscosity and sedimentation study of sonicated DNA–proflavine complexes, Biopolymers 8 (1969) 45–55, https://doi.org/10.1002/bip.1969.360080105.
[32] T.A. Fairley, R.R. Tidwell, I. Donkor, N.A. Naiman, K.A. Ohemeng, R.J. Lombardy, J.A. Bentley, M. Cory, Structure, DNA Minor Groove Binding, and Base Pair Specificity of Alkyl- and Aryl-Linked Bis(amidinobenzimidazoles) and Bis (amidinoindoles), J. Med. Chem. 36 (1993) 1746–1753, https://doi.org/10.1021/jm00064a008.
[33] P.B. Gratal, J.G. Quero, A. Pérez-Redondo, Z. Gándara, L. Gude, PhenQE8, a Novel Ligand of the Human Telomeric Quadruplex, Int. J. Mol. Sci. 22 (2021) 749, https://doi.org/10.3390/ijms22020749.
[34] W. Paw, R. Eisenberg, Synthesis, Characterization, and Spectroscopy of Dipyridocatecholate Complexes of Platinum, Inorg. Chem. 36 (1997) 2287–2293, https://doi.org/10.1021/ic9610851.
[35] [a] S.S. Qasim, S.S. Ali, S.K. Ahmed, SnCl2.2H2O catalyzed one-pot synthesis of 2-phenylimidazo[4,5-f][1,10]phenanthroline, Res. J. Pharm. Biol. Chem. Sci. (RJPBCS) 2 (2011) 423–428;
[b] S.S. Ali, An efficient synthesis of 2-phenylimidazo[4,5-f][1,10]phenanthroline derivatives catalysed by boric acid under solvent free conditions at room temperature, Org. Chem.: Indian J. 7 (2011) 270–274;
[c] S.S. Ali, One-pot synthesis of 2-phenylimidazo[4,5-f][1,10]phenanthroline derivatives under solvent free conditions by using iodine, Arch. Appl. Sci. Res. 2 (2010) 392–397.
[36] D. Sehnal, S. Bittrich, M. Deshpande, R. Svobodová, V. Karel Berka, S. Bazgier, S. K. Velankar, J. Burley, A.S.R. Koca, Mol* Viewer: modern web app for 3D visualization and analysis of large biomolecular structures, Nucl. Acids Res. 49 (2021) W431–W437, https://doi.org/10.1093/nar/gkab314.
[37] J. Dai, M. Carver, C. Punchihewa, R.A. Jones, D. Yang, Structure of the Hybrid-2 type intramolecular human telomeric G-quadruplex in K^+ solution: insights into structure polymorphism of the human telomeric sequence, Nucleic Acids Res. 35 (2007) 4927–4940, https://doi.org/10.1093/nar/gkm522.